論文 / 著書情報
Article / Book Information

Title	Comparative Analysis of Future Urban Thermal Comfort in Three Cities Considering Urbanization Under Multiple CMIP6 Scenarios
Authors	Xiao Jin, Alvin C. G. Varquez, Do Ngoc Khanh, Tomohiko Ihara, Norihiro Itsubo, Manabu Kanda, I. Dewa Gede Agung Junnaedhi
Citation	Earth and Space Science, Vol. 13, Issue 7,
Pub. date	2026, 7
DOI	https://doi.org/10.1029/2025EA004856
Creative Commons	Information is in the article.

ADVANCING EARTH AND SPACE SCIENCES

Earth and Space Science

RESEARCH ARTICLE
10.1029/2025EA004856

Special Collection:
Advancing Multi-Decadal Climate Projections for Societally Relevant Applications

Key Points:

- Future rise in near-surface air temperature and thermal comfort were projected for three megacities under varying climate-change forcings
- Intercity and intracity variability are moderated by background climate conditions and spatially-varying urbanization levels, respectively
- Urbanization-modified thermal comfort depends not on air-temperature rise, but also on other meteorological factors, season, and geography

Supporting Information:

Supporting Information may be found in the online version of this article.

Correspondence to:

X. Jin,
jin.x.9a30@m.isct.ac.jp

Citation:

Jin, X., Varquez, A. C. G., Khanh, D. N., Ihara, T., Itsubo, N., Kanda, M., & Junnaedhi, I. D. G. A. (2026). Comparative analysis of future urban thermal comfort in three cities considering urbanization under multiple CMIP6 scenarios. *Earth and Space Science*, *13*, e2025EA004856. https://doi.org/10.1029/2025EA004856

Received 24 OCT 2025
Accepted 24 JUN 2026

Author Contributions:

Conceptualization: Xiao Jin, Alvin C. G. Varquez
Formal analysis: Xiao Jin, Alvin C. G. Varquez

Comparative Analysis of Future Urban Thermal Comfort in Three Cities Considering Urbanization Under Multiple CMIP6 Scenarios

Xiao Jin[1], Alvin C. G. Varquez[1], Do Ngoc Khanh[2], Tomohiko Ihara[3], Norihiro Itsubo[4], Manabu Kanda[1], and I. Dewa Gede Agung Junnaedhi[5]

[1]Department of Transdisciplinary Science and Engineering, School of Environment and Society, Institute of Science Tokyo, Tokyo, Japan, [2]SIT Research Laboratories, Shibaura Institute of Technology, Tokyo, Japan, [3]Department of Environment Systems, Graduate School of Frontier Sciences, The University of Tokyo, Kashiwa, Japan, [4]Department of Science and Engineering, School of Creative Science and Engineering, Waseda University, Tokyo, Japan, [5]Atmospheric Sciences Research Group, Faculty of Earth Sciences and Technology, Institut Teknologi Bandung, Bandung, Indonesia

Abstract This work investigates variations in thermal conditions in cities with different background climates exposed to climate change and future urbanization (i.e., horizontal/vertical urban expansion and energy consumption change). Simultaneously considering projected urbanization from the present to the 2050s, characterized by spatial changes in urban parameters and anthropogenic heat emissions (AHE), 1.5-km present and future climates of Tokyo, Cairo, and Jakarta in the 2050s were modeled using initial and boundary conditions from the National Centers for Environmental Prediction Global Data Assimilation System/Final (NCEP GDAS/FNL) 0.25° Global Tropospheric Analyses and Forecast Grids and Coupled Model Intercomparison Project Phase 6 (CMIP6) climate-change scenarios based on Shared Socioeconomic Pathways (SSP126, SSP245, and SSP370). The Universal Thermal Climate Index (UTCI) was estimated using the UTCI-Fiala model. Regional near-surface air temperature and UTCI scaled proportionally with background climate changes. Projected urbanization caused significant intra-urban variability, with some locations showing warming comparable to background climate change. It also altered strong heat-stress exposure, defined as hours with UTCI > 32 °C, amplifying exposure in Cairo and Jakarta but slightly offsetting it in Tokyo, where AHE declined. Cities with different background climates exhibited distinct seasonal responses: Tokyo showed moderate bimodal variability, Cairo exhibited the strongest variability with peak summer warming, and Jakarta showed a uniform increase year-round. Near-surface air temperature and UTCI responses to urbanization also varied seasonally across scenarios and cities, while variables beyond air temperature contributed to thermal-comfort changes. This study strengthens the necessity of projecting not only meteorology, but also socially relevant indices, such as UTCI.

Plain Language Summary Climate change is making cities hotter, and urbanization can further change how heat is experienced. This work uniquely considers site-specific urbanization in terms of horizontal/vertical urban expansion and anthropogenic heat emission changes. We conducted high-resolution numerical simulations to quantify present and 2050s spatiotemporal outdoor heat stress in Tokyo, Cairo, and Jakarta, each having unique background climates and urbanization levels. Heat stress was assessed using the Universal Thermal Climate Index (UTCI), a "feels-like" temperature that considers air temperature, humidity, wind, and radiation. We found that climate change increases both air temperature and UTCI, but UTCI often rises more, meaning people may feel hotter than air temperature alone suggests. The changes differed by city: Cairo showed the strongest summer increase, Tokyo showed two seasonal peaks, and Jakarta increased more steadily year-round. In some neighborhoods, urbanization effects were comparable to background climate change. Urbanization also increased hours of strong heat stress in Cairo and Jakarta, but slightly reduced them in Tokyo, where human heat release declined. These results show that future urban heat risk cannot be assessed from air temperature alone and that urban planning can influence future heat exposure.

1. Introduction

The interplay between global warming and urbanization raises a critical challenge for human society (Castells-Quintana et al., 2021; Helbling & Meierrieks, 2023; McCarthy et al., 2010; Moazzam et al., 2022; Wang et al., 2023). According to the Intergovernmental Panel on Climate Change (IPCC), global mean temperatures

Funding acquisition: Alvin C. G. Varquez, Tomohiko Ihara
Investigation: Xiao Jin
Methodology: Xiao Jin, Alvin C. G. Varquez, Do Ngoc Khanh
Resources: Alvin C. G. Varquez
Supervision: Alvin C. G. Varquez, Manabu Kanda
Writing – original draft: Xiao Jin
Writing – review & editing: Alvin C. G. Varquez, Do Ngoc Khanh, Tomohiko Ihara, Norihiro Itsubo, Manabu Kanda, I. Dewa Gede Agung Junnaedhi

have risen, on average, by 1.1°C since preindustrial times, with the urban heat island effect amplifying warming in cities (IPCC, 2021). Currently, 55% of the global population, about 4.4 billion people, reside in urban areas, a share projected to reach 68% by 2050s (UN DESA, 2018), thus increasing exposure and vulnerability to climate-related risks (Lankao & Qin, 2011). As cities face compounded atmospheric-related impacts from climate change and urbanization, understanding urban-climate dynamics is increasingly critical, particularly in rapidly developing regions (Leal Filho et al., 2019; X. Li et al., 2022; Macagba & Delina, 2024).

Urban areas account for approximately 70% of global carbon emissions and face disproportionate climate impacts, prompting the IPCC to emphasize the urgency of implementing urban climate action (Solecki et al., 2024). Early climate model investigations using global climate models (GCMs) mainly provided large-scale climate projections. However, most GCMs do not explicitly represent urban areas, and their coarse spatial resolution prevents them from resolving urban heat island effects or intra-urban heterogeneity (Zhang et al., 2023; L. Zhao et al., 2021). While regional downscaling approaches have improved spatial detail in acquiring future thermal comfort projections (Shukla & Attada, 2023), most studies examine either climate change or urbanization effects separately, with assessments of their inseparable and compounding impacts on various urban thermal environments still limited (Chapman et al., 2017; Kusaka et al., 2012; Yuan et al., 2022; Y. Zhao et al., 2021). Studies that treat urbanization as a function not only of land cover change (i.e., urban expansion) but also changes in urban morphology and anthropogenic heating under multiple climate-change scenarios are still lacking. Although recent studies have incorporated urbanization into climate projections (Darmanto et al., 2019; Khanh et al., 2023), systematic investigations of coupled climate-urbanization responses under diverse urban forms and climatic backgrounds on thermal comfort are still needed. Adequate consideration of urbanization effects in future climate projections given diverse cities is a crucial primary step to develop effective adaptation and mitigation strategies (Goodess et al., 2021; Hamdi et al., 2020). For clarity, urbanization, as investigated in this study, is defined as encompassing horizontal urban expansion (i.e., land-cover change), vertical urban expansion, and energy-consumption changes represented by anthropogenic heat emissions (AHE).

Applied urban-climate research focusing on human-centered thermal comfort has shifted from solely depending on air temperature in quantifying heat stress to other integrated indices (Epstein & Moran, 2006; Höppe, 2002; Y. Li et al., 2025; Martilli, Nazarian, Krayenhoff, Lachapelle, et al., 2024; Nazarian et al., 2022; Ren et al., 2022; Zhang et al., 2023). Contemporary studies have developed various thermal comfort indices (Gulyás et al., 2006; Jendritzky et al., 2012; Lai et al., 2020). Among them is the Universal Thermal Climate Index (UTCI), which provides a physiologically based assessment of thermal stress using a multi-node model that incorporates air temperature, wind speed, humidity, and radiation (Fiala et al., 2012; Jendritzky et al., 2012). Compared to other empirical indices such as the Heat Index or the Wet Bulb Globe Temperature, UTCI offers a more comprehensive evaluation, particularly in outdoor environments (Blazejczyk, 1994; Blazejczyk et al., 2012). UTCI is also accompanied by standardized categories of thermal stress, facilitating consistent comparisons across diverse climatic contexts (Fiala et al., 2012; Jendritzky et al., 2012). This is particularly relevant given that outdoor thermal comfort varies significantly by region, as revealed by field surveys and observation-based analyses across diverse climates (S. Liu et al., 2022; Wu et al., 2019). Tropical cities possess unique seasonal dynamics and require tailored heat mitigation strategies (Roth, 2007; Santamouris et al., 2015), while arid cities commonly exhibit pronounced day–night comfort contrasts due to low humidity and intense solar radiation (Giridharan & Emmanuel, 2018).

With the growing adoption of UTCI as a measure of outdoor thermal comfort, an increasing number of studies have explicitly examined its response to climate change in urban environments (Briegel et al., 2025; Hiroki et al., 2025; Hundhausen et al., 2023; Paranunzio et al., 2021; Weeding et al., 2024). However, these studies assume a static urban form or represent future urbanization only in broad terms (i.e., through local climate zone classifications) (Briegel et al., 2025; Hundhausen et al., 2023; Paranunzio et al., 2021; Weeding et al., 2024), leaving the effects of explicit future urbanization, which encompasses changes in land cover, urban morphology, and AHE, insufficiently explored. On the other hand, studies that simultaneously consider future climate change and detailed future urbanization have largely relied on near-surface air temperature as a proxy for thermal comfort (Darmanto et al., 2019; Khanh et al., 2023; A. C. G. Varquez, Darmanto, et al., 2020), which cannot fully describe the human physiological response (i.e., days of similar air temperatures but different humidity levels may lead to significant differences in thermal comfort).

To address these gaps, this study aims to investigate future outdoor thermal comfort using UTCI, explicitly accounting for future urbanization from the present to the 2050s—encompassing spatial changes in land cover, urban morphology, and AHE—together with climate change across cities with contrasting climatic backgrounds, thereby providing new insights into this underexplored area. This is made possible by recent advances in urban climate modeling. Climate projections over cities require future background and surface scenarios, as well as appropriate climate-model parameterizations that can consider spatial variability in urban representations. Global climate models (GCMs), such as those used in Coupled Model Intercomparison Project Phase 6 (CMIP6), feature improved resolution and representation of physical processes, providing a wider and reliable range of plausible projections than those used in previous intercomparisons (Eyring et al., 2016; Gier et al., 2024; O'Neill et al., 2016; Taylor et al., 2012). GCM projections may be downscaled over cities using regional climate models, such as the Weather Research and Forecasting (WRF) model (Skamarock & Klemp, 2008), and the Pseudo-Global Warming (PGW) method (Giorgi & Mearns, 1991; Kimura & Kitoh, 2007; Powers et al., 2017). In recent WRF versions, integrated WRF/urban modeling system capable of representing spatiotemporal heterogeneities in urban parameters and anthropogenic heating have become available (F. Chen et al., 2011; Kanda et al., 2013; Kusaka et al., 2001; Martilli, 2007; Martilli et al., 2002; Masson et al., 2002; Salamanca et al., 2011; A. C. Varquez et al., 2015, 2021).

Urban canopy schemes differ substantially in complexity (F. Chen et al., 2011; Karlický et al., 2018). Bulk schemes are efficient but treat cities as effective surfaces without explicit geometry (Karlický et al., 2018). Single-layer urban canopy models, such as WRF-SLUCM, represent idealized canyon-scale roof, wall, and road energy exchanges at moderate computational cost, but rely on simplified canyon geometry (X. He et al., 2019; Kusaka et al., 2001). Multi-layer schemes, such as the Building Effect Parameterization coupled with a Building Energy Model (BEP-BEM), represent vertical canopy structure and vertically distributed building–atmosphere exchanges, but require more detailed morphology and building inputs (Ao et al., 2024; F. Chen et al., 2011; Y. Liu et al., 2006; Martilli et al., 2002; Salamanca et al., 2010). Building-resolving computational fluid dynamics/large-eddy simulation (CFD/LES) models resolve individual buildings and turbulence, but their computational, data, and inflow-boundary requirements limit long-term, multi-city climate applications (S. Qin et al., 2025; Teng et al., 2025; Toparlar et al., 2017). In this study, the WRF-SLUCM model is adopted given its practical balance between physical realism and computational efficiency for regional multi-city simulations. This choice is further motivated by the availability of present and future urban data sets, encompassing land cover change, urban morphological parameters, and AHE (Khanh et al., 2021, 2023; A. C. Varquez et al., 2021), and enabling explicit representation of future urbanization across the 2010s and 2050s.

Building on this, this study further aims to:

- investigate the spatiotemporal thermal comfort (i.e., UTCI) responses to climate-change forcings and future urbanization across three cities with different climate backgrounds and urbanization levels;
- project future urban climate and thermal comfort in the 2050s considering urbanization under three CMIP6 scenarios;
- explore discrepancies between near-surface air temperature (2 m air temperature above the surface, T2) and UTCI responses to future urbanization and determine the key meteorological drivers influencing the UTCI response.

Here, three megacities representing diverse climate zones and urbanization levels were selected, namely: Tokyo (Japan), Cairo (Egypt), and Jakarta (Indonesia). Hourly meteorology and UTCI at 1.5 km resolution were modeled and analyzed for a full-year period under varying background climate conditions. The details of this procedure and its underlying assumptions are explained in the following section.

2. Methodology

In this section, the climate simulation settings, the UTCI assessment, and the attribution analysis method are described. Attribution analysis quantifies the relative contribution of meteorological changes induced by projected urbanization to variations in UTCI under different CMIP6 scenarios.

10.1029/2025EA004856

2.1. Target Cities and Periods

The selected megacities were Tokyo, Cairo, and Jakarta, experiencing temperate (Cfa), arid (BWh), and tropical monsoon (Am) climates (Peel et al., 2007), respectively. Each city represents varying socio-economic development and urbanization stages, from fully developed to rapidly expanding megacities (Darmanto et al., 2019; S. M. Robaa, 2013; Seto et al., 2012; UN DESA, 2018). The base period for the present climate simulations was the year 2022. In this La Niña year, various areas worldwide experienced record-breaking hot weather conditions and witnessed numerous extreme weather events (Blunden & Boyer, 2023; NOAA Climate.gov, 2023). As the basis for future climate simulations, three CMIP6 scenarios (O'Neill et al., 2016) were selected: SSP126 (low-emission, sustainability-focused), SSP245 (intermediate), and SSP370 (high-emission, fossil-fuel-intensive) (Fricko et al., 2017; Fujimori et al., 2017; Riahi et al., 2017).

2.2. Weather Simulation Settings

Three-domain one-way nested WRF simulations (Powers et al., 2017; Skamarock & Klemp, 2008) were conducted for the entire year of 2022 and a representative year of the 2050s. Centered on each selected megacity, the innermost horizontal resolution and output history intervals were set to 1.5 km (Figure S1 in Supporting Information S1) and hourly, respectively. Land cover classification of the study areas under the present-day urban configuration is shown in Figure 1a.

WRF v4.6, enabling a modified (Kanda et al., 2013; Khanh et al., 2023) single-layer urban canopy model (SLUCM, Kusaka et al., 2001) was used, which enables spatially-heterogeneous representations of present and 2050s urban parameters (i.e., roughness length, displacement height, frontal area index, mean building height, plan area index, AHE). The urban parameter distributions were obtained from the work of Khanh et al. (2023) and downloaded from Khanh et al. (2021). The hourly-changing AHE used was the AH4GUC data set (A. C. Varquez et al., 2021). The spatial distributions of present-day (2020s) urban conditions and projected changes for the 2050s across the three target cities are shown in Figure 1b. Here, only the mean building height (H_{avg}) and AHE are shown. Other urban parameters, such as plan area index (λ_p), frontal area index $\left(\lambda_f\right)$, roughness length (Z_0), and zero-plane displacement height (Z_d), were also modified (see Figure S3 in Supporting Information S1). The present distributions reveal pronounced spatial heterogeneity in both urban morphology and AHE within each city. Projected changes indicate more noticeable increases in mean building height in Jakarta and Cairo, whereas changes in Tokyo are minimal. In Jakarta, increases tend to extend from the urban core toward surrounding sectors of the domain, suggesting spatially heterogeneous urbanization consistent with previous urban growth projections for Jakarta (Darmanto et al., 2019; A. C. Varquez et al., 2017). Changes in AHE also differ among the cities, with an overall decrease in Tokyo but projected increases in Jakarta and Cairo. To ensure consistency among simulations, the same physical parameterization schemes and common numerical settings, following previous studies (Darmanto et al., 2019; Khanh et al., 2023; A. C. Varquez et al., 2015), were adopted and are summarized in Table S1 in Supporting Information S1.

Meteorological inputs for the present-day simulations were obtained from the 0.25° NCEP GDAS/FNL operational global analyses and forecast grids (National Centers for Environmental Prediction, National Weather Service, NOAA, U.S. Department of Commerce, 2015). These fields were used to provide the initial and lateral boundary conditions for the WRF simulations (Powers et al., 2017). Future climate boundary conditions were generated using the pseudo-global-warming (PGW) approach (Brogli et al., 2023; Giorgi & Mearns, 1991; Kimura & Kitoh, 2007), a dynamical downscaling strategy in which climatological climate-change signals (i.e., deltas between future and present climates derived from GCMs) are superimposed onto present-day reanalysis fields to construct perturbed initial and boundary conditions. This approach preserves the synoptic variability and event chronology of the reanalysis while incorporating projected thermodynamic changes by modifying atmospheric initial and lateral boundary conditions rather than directly using raw GCM outputs. These modifications are typically applied to three-dimensional atmospheric variables (e.g., temperature, wind, and humidity) as well as key surface variables (e.g., 2-m air temperature, near-surface relative humidity (RH2), sea surface temperature, and surface skin temperature). In this study, the PGW deltas were calculated as monthly climatological differences between the mid-century (2045–2054) and present (2015–2024) periods. The final PGW ensemble was constructed from CMIP6 models with complete ScenarioMIP monthly data for the required variables, SSP scenarios, native-grid data, and analysis periods (Table S2 in Supporting Information S1). These PGW deltas were then applied to both three-dimensional atmospheric fields and surface variables. The PGW4ERA5 v1.1

10.1029/2025EA004856

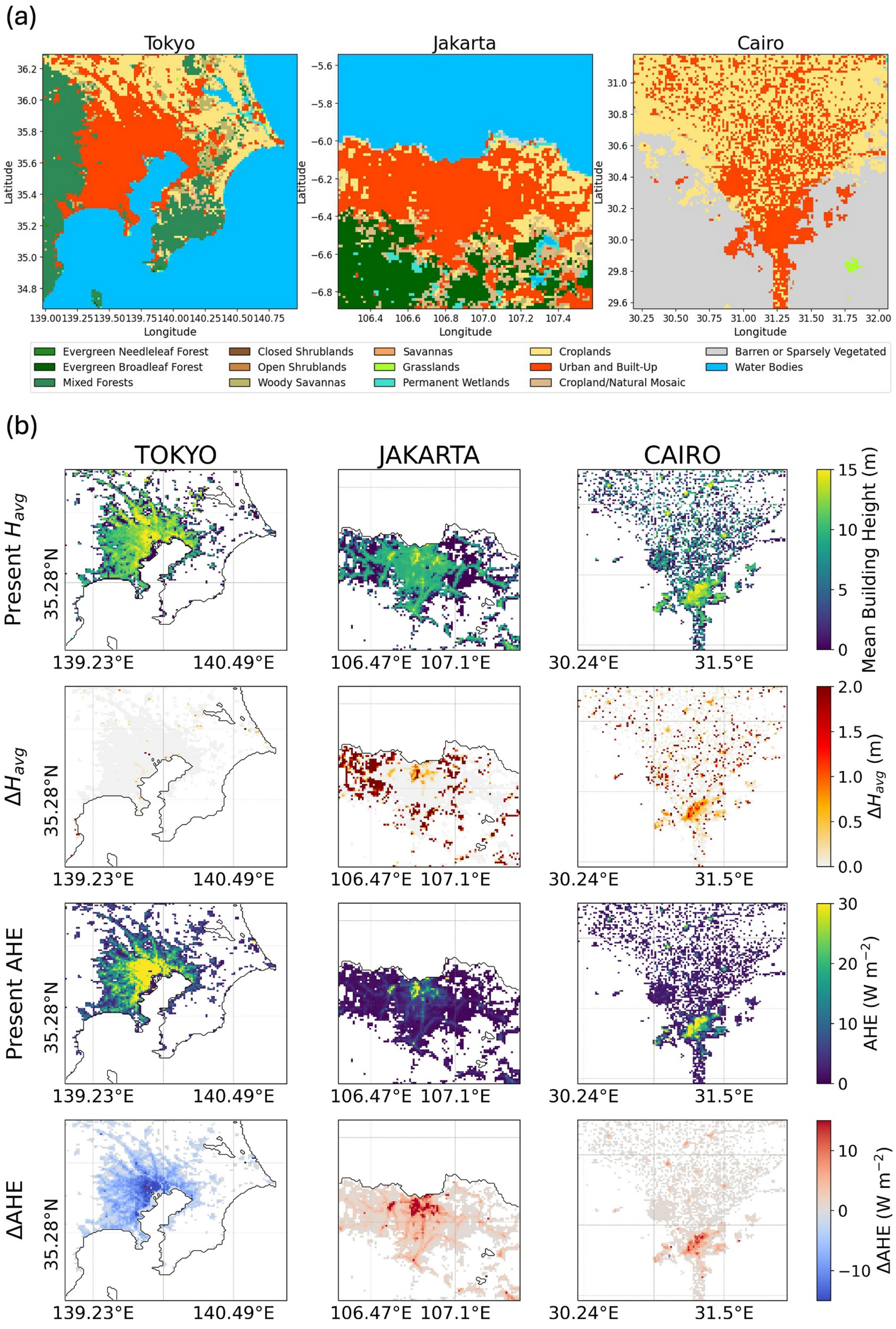

Figure 1. Study areas. (a) Land cover classification of the study areas under the present-day urban configuration (PU). "Urban and Built-Up" grid cells (orange) define the urban mask, and all analyses are restricted to these present urban grids to ensure spatial consistency. (b) Spatial distributions of present (2020s) urban conditions and projected changes for the 2050s. Mean building height (H_{avg}) and anthropogenic heat emissions are shown as examples.

workflow (Brogli et al., 2023) was adapted to generate WRF-compatible forcing by merging ensemble-averaged CMIP6 deltas (r1i1p1f1) with the 2022 NCEP GDAS/FNL baseline. Deltas were bilinearly interpolated to the FNL/WRF forcing grid, temporally averaged to monthly means, and applied to adjust three-dimensional atmospheric fields (temperature, horizontal wind, geopotential) and surface variables (2-m temperature, 2-m RH2, sea surface temperature, and surface skin temperature).

For each city, seven simulations were performed using combinations of (a) climate forcing (baseline NCEP GDAS/FNL forcing for 2022 and PGW-based future forcings under SSP126/SSP245/SSP370) and (b) urban surface configuration (present-day urban configuration, PU; and projected 2050s urban configuration, FU). Specifically, the seven scenarios are:

- P: present-day urban configuration with NCEP GDAS/FNL (2022) boundary conditions;
- PU1–PU3: present-day urban configuration forced by SSP126, SSP245, and SSP370 boundary conditions;
- FU1–FU3: projected (2050s) urban configuration forced by SSP126, SSP245, and SSP370 boundary conditions.

The effect of projected urban configuration change is defined as $\Delta UP = FU - PU$ under identical climate forcing, where UP denotes the set of urban parameters (e.g., urban morphology and AHE) that differ between the present-day and 2050s urban data sets. This study was carried out using the TSUBAME4.0 supercomputer at Institute of Science Tokyo (Endo et al., 2023).

2.3. Thermal Comfort Estimation

As mentioned in Section 1, UTCI was selected to assess outdoor thermal comfort. We used the empirical approximation (Bröde et al., 2012), which closely reproduces the UTCI–Fiala model (Fiala et al., 2012; Havenith et al., 2012) at reduced computational cost. The four variables required for the computation of the UTCI—2-m air temperature (T2), 2-m RH2, 10-m wind speed (U10), and mean radiant temperature (T_{mrt})—were obtained from the hourly WRF model outputs. UTCI was calculated at an hourly time step using these variables, and the monthly UTCI values presented in this study were derived by averaging the hourly UTCI values. T_{mrt} was calculated based on the approach of Di Napoli et al. (2021) utilizing the simulated downward shortwave radiation, downward longwave radiation, surface albedo, surface emissivity, and skin temperature. These were combined into a net radiative forcing following the Stefan–Boltzmann law, incorporating direct, diffuse, and reflected shortwave radiation, as well as surface and sky longwave radiation (see Text S2 and Table S3 in Supporting Information S1 for the full formulation).

This work assumed a simplified approach for the T_{mrt} on the basis that the radiation-relevant variables implicitly contain the urban effect through urban parameterization. Also, spatially resolving radiative temperatures in urban canopy models remains uncertain (Schoetter et al., 2023). While this simplified treatment is practical for mesoscale scenario simulations, the resulting T_{mrt}, wind speed, and thus UTCI remain limited in representing pedestrian-level microclimatic conditions at 1.5-km resolution; the methodological limitations of mesoscale UTCI modeling are discussed more critically in Section 3.5.

2.4. Quantifying the Relative Importance of the Projected Urbanization-Induced Changes in the Meteorological Drivers to the Changes in the UTCI Through Machine Learning

The UTCI regression equation is highly non-linear and complex (Bröde et al., 2012), making it difficult to directly infer the relative importance or influence of individual meteorological variables on thermal comfort. In this work, we used the Light Gradient Boosting Machine (LightGBM) framework to evaluate the feature importance of the variables affecting the UTCI. LightGBM can capture complex, nonlinear relationships and feature interactions compared to other conventional models (Ke et al., 2017) and has demonstrated strong capabilities in modeling environmental variable interactions (C. Li et al., 2025; C. Zhao et al., 2025).

In this study, the focus was mainly on the projected urbanization-induced UTCI change, ΔUTCI(ΔUP), computed as the difference between paired future-urban (FU) and present-urban (PU) runs under the same CMIP6 scenario, using grid-level monthly means. The features that were fed into the LightGBM included the present-day states and the projected urbanization-induced changes of the influential near-surface meteorological variables to the UTCI. The baseline predictors were the climate-forcing-induced changes in $T2$, $RH2$, $U10$, and T_{mrt}, quantified as $\Delta T2$ (PU − P), $\Delta RH2$ (PU − P), $\Delta U10$ (PU − P), and ΔT_{mrt} (PU − P) under fixed present-day urban conditions.

These variables represent the background meteorological shifts attributable to climate forcing alone and therefore provide the baseline against which the additional impact of future urban development is evaluated. Its projected urbanization-induced changes are denoted by $\Delta T2(\Delta UP)$, $\Delta RH2(\Delta UP)$, $\Delta U10(\Delta UP)$, $\Delta T_{mrt}(\Delta UP)$, respectively. Separate LightGBM models were trained for each city and seasonal subset (wet/dry for Jakarta; spring, summer, autumn, winter for Tokyo and Cairo) under each climate scenario. For each city–season–scenario subset, the data were split into training (≈70%), validation (≈20%), and independent testing (≈10%) sets. The full model settings are found in Table S4 in Supporting Information S1.

Feature importance was quantified using *Gain*, defined as the cumulative improvement in model performance (loss reduction) attributed to each variable across all decision trees; values are unitless and should be interpreted in relative terms, where larger values indicate higher predictive importance (Ke et al., 2017).

3. Results and Discussion

3.1. Model Evaluation

Simulated hourly 2 m air temperature (T2) was evaluated against 2022 in situ observations from meteorological stations compiled in the Tokyo, Jakarta, and Cairo domains using the NOAA Integrated Surface Database (Smith et al., 2011). Monthly normalized Taylor diagrams (Figure S4 in Supporting Information S1) summarize correlation, normalized standard deviation, and centered RMSE across months. Across all station–month pairs, T2 RMSE ranged from 1.23 to 4.62°C (median 2.42°C; 22 stations, 240 station–month pairs) in Tokyo, 1.42–3.39°C (median 2.04°C; 6 stations, 69 station–month pairs) in Jakarta, and 1.76–3.04°C (median 2.20°C; 1 station, 12 station–month pairs) in Cairo, with corresponding mean-bias ranges of −3.58–2.72 °C, −2.85–0.01 °C, and −1.28–−0.65 °C, respectively. Month-specific performance shows that Cairo maintains consistently high correlation throughout the year ($r = 0.904$–0.967), with RMSE lowest in February (1.76°C) and highest in July (3.04°C), while the normalized standard deviation remains > 1, indicating systematically over-amplified variability. Jakarta exhibits stronger month-to-month variability: monthly median RMSE spans 1.57°C in June (1.48°C–2.39°C) to 2.35°C in April (1.60°C–3.32°C), and monthly median correlation increases from ∼0.58 in February (0.40–0.71) to ∼0.82 in August (0.78–0.88); most months show damped variability.

Following Oreskes et al. (1994), we interpret these results in an adequacy-for-purpose sense rather than as formal validation. We define an application-specific performance threshold following the benchmarking principle that performance expectations should be tied to intended use (Best et al., 2015). Although the present evaluation focuses on T2, as radiation flux observations required for the calculation of T_{mrt} were not available across the study domain, T2 is a primary driver of UTCI and its accurate simulation is essential for reliable UTCI estimation. Because UTCI heat-stress categories are ∼6°C wide (Bröde et al., 2012), within which an uncertainty of one full category width has been considered acceptable for biometeorological applications (Weihs et al., 2012), we adopt a conservative threshold of T2 RMSE <∼3°C (approximately half of a category width) as a practical, use-case-informed benchmark. It is acknowledged that the full uncertainty in modeled UTCI would additionally incorporate errors in wind speed, humidity, and radiation-derived T_{mrt}, and therefore remains unquantified in the present study.

Tokyo shows generally comparable median errors (median RMSE: 2.42°C), but with a wider range (1.23°C–4.62°C). Exceedances of the ∼3 °C threshold occur in multiple months (e.g., April–July, September, and December), involving a subset of stations rather than uniformly across the domain. In these months, exceedances are typically limited to several stations (generally 2–5 stations per month), while the majority of stations remain below the threshold. Notably, the exceedances are not randomly distributed but tend to recur at specific stations, including Chichibu, Tokyo Heliport, Chofu Airport, Tateyama, Shimofusa, and Oshima, indicating systematic site-dependent biases rather than domain-wide model deficiencies.

Jakarta exhibits greater variability across months, with monthly median RMSE ranging from 1.57°C to 2.35°C and overall values spanning 1.42°C–3.39°C. Exceedances of the ∼3 °C threshold occur in several months (e.g., March–April, July, and November–December), involving a subset of stations rather than uniformly across the domain. In these months, exceedances are primarily associated with specific stations, most notably Halim Perdanakusuma International Airport, which shows repeated exceedances across multiple months, and to a lesser extent Soekarno Hatta International Airport. In contrast, other stations generally remain below the threshold, indicating that model errors are spatially heterogeneous and dominated by site-specific biases.

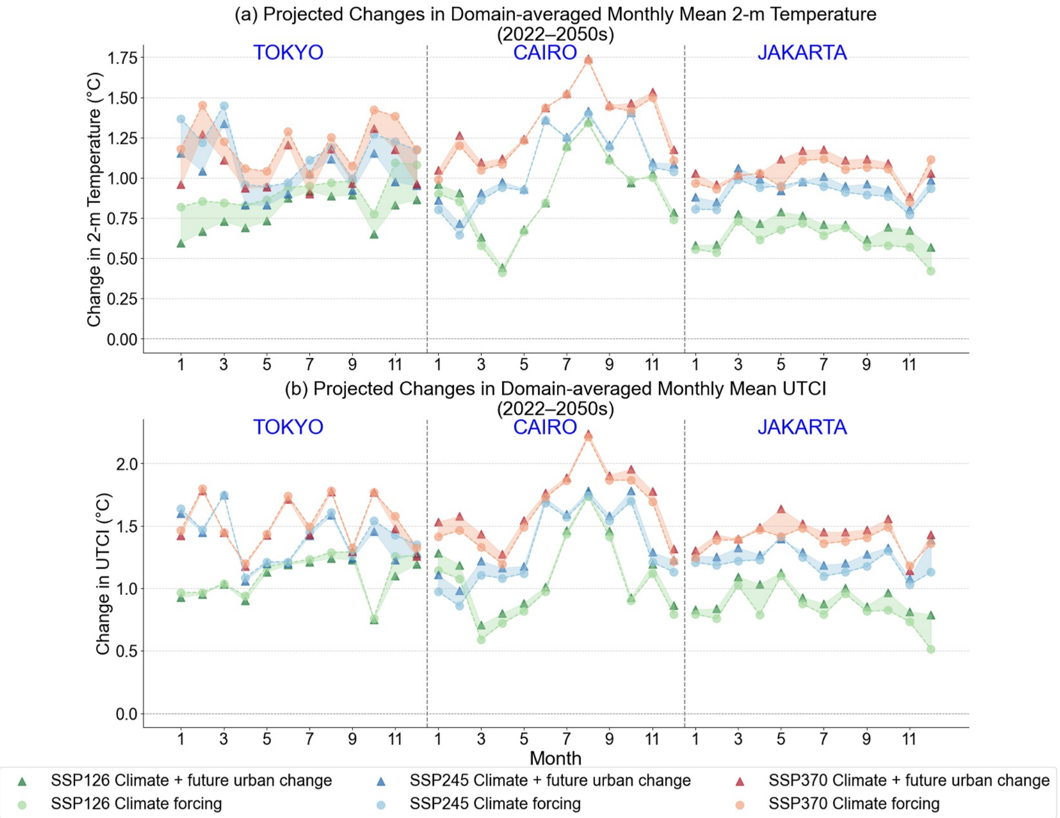

Figure 2. Future changes (2022–2050s) in spatially averaged monthly T2 (a) and Universal Thermal Climate Index (b) across cities and scenarios. Triangles show $FU - P$ (combined effect of future climate forcing and projected urban configuration change relative to the baseline). Circles show $PU - P$ (effect of future climate forcing relative to the baseline, with the urban configuration held at present-day values). The shaded area between the two curves represents the additional contribution of projected urban configuration change ($FU - PU = \Delta UP$). Colors denote SSP126/SSP245/SSP370. Calculations were based on the urban area in 2022.

Cairo maintains consistently high performance throughout the year ($r = 0.904$–0.967), with RMSE ranging from 1.76°C to 3.04°C. Only a single exceedance of the ∼3 °C threshold is observed in July (3.04°C), while all other months remain below the threshold, indicating stable and consistent model performance without systematic site-dependent biases.

In addition, time-series comparisons between simulations and observations are included (Figure S5 in Supporting Information S1) to complement the summary error metrics and provide additional insight into the temporal characteristics of model errors.

3.2. Citywide Monthly Responses of UTCI and $T2$ to Future Climate Forcing and Urbanization

To attribute changes in $T2$ and UTCI to background climate forcing versus projected urbanization, we compare three simulations defined in Section 2.2: P (baseline 2022 NCEP GDAS/FNL forcing with present-day urban configuration), PU (future SSP forcing with present-day urban configuration), and FU (future SSP forcing with projected 2050s urban configuration). For a given SSP scenario, $PU - P$ quantifies the effect of background climate forcing relative to the baseline while holding the urban configuration fixed at present-day values. $FU - P$ represents the combined effect of background climate forcing and projected urban configuration change. The difference $FU - PU$ ($= \Delta UP$) isolates the conditional effect of projected urban parameter changes (i.e., land cover, urban morphology, and AHE) under the same future climate forcing.

By 2050, $T2$ and UTCI are projected to increase in Tokyo, Cairo, and Jakarta across all scenarios, with UTCI increases consistently exceeding $T2$ warming (Figure 2). Spatially-averaged monthly $T2$ are projected to increase by approximately 0.6°C–1.5°C in Tokyo, 0.4°C–1.8°C in Cairo, and 0.4°C–1.2°C in Jakarta. Corresponding

UTCI increases are projected to be about 0.75–1.78°C, 0.6–2.25°C, and 0.5–1.63°C, respectively. At the regional scale, climate forcing dominates the projected increase in both $T2$ and UTCI, with SSP370 producing roughly 1.5–2× greater warming than SSP126. At the local scale, projected urbanization (ΔUP) introduces spatial heterogeneity in the $T2$ and UTCI, with a few hotspots within Cairo and Jakarta (Figure S7 in Supporting Information S1) that manifest increases in magnitude similar to those caused by background climate-change forcing (Figure 2). As will be discussed later in Section 3.4, the location of the hotspots, such as in Jakarta, may vary for both $T2$ and UTCI under specific conditions.

In terms of seasonal changes, Cairo shows the strongest seasonality, with summer $T2$ increases peaking near 1.8°C and UTCI around 2.25°C under SSP370, while SSP126 exhibits pronounced summer peaks (∼1.3°C–1.4°C for $T2$; ∼1.7°C–1.8°C for UTCI). Although having similar seasonality patterns, SSP245 shows a relatively milder August maximum, comparable to June and October. Tokyo exhibits moderate seasonal variability. Under SSP245 and SSP370, $T2$ follows a bimodal pattern with higher warming during the peak of winter (February) and in the mid-autumn (October and November), with relatively lower increases during the spring and summer months. A similar bimodal pattern can also be found for the UTCI in SSP245. In SSP126, warming is more uniform, with a peak during summer and a minimum in early autumn. Jakarta shows minimal seasonality, consistent with its equatorial monsoon climate (Darmanto et al., 2019; Paramita & Matzarakis, 2023). SSP126 shows slightly weaker warming in November–December than SSP245 and SSP370 (Figure 2). This stronger seasonality in Cairo likely reflects differences in background climate. Cairo is characterized by hot-arid, predominantly clear-sky conditions and relatively weak cloud attenuation of incoming shortwave radiation (S. Robaa, 2006). In contrast, the warm season in Japan includes a low-sunshine Baiu period (Inoue & Matsumoto, 2003), and summertime temperatures in the Tokyo metropolitan area are further modulated by sea-breeze penetration (Yamato et al., 2017). These factors can suppress warm-season T2 increases in Tokyo, whereas under future climate forcings the projected T2 signal in Cairo is superimposed on a background state with stronger seasonal radiative contrast, producing a more pronounced summer maximum. The similar monthly evolution of UTCI and T2 suggests that, under future climate forcings, both metrics exhibit broadly similar seasonal responses, and may therefore be interpreted consistently.

The impact of projected urbanization on spatially averaged monthly UTCI and near-surface air temperature across cities and scenarios is summarized in Figure 2 and Figure S6 in Supporting Information S1. Colder months tend to have larger UTCI and $T2$ increases due to future urbanization. Consistent with previous studies (B. Chen et al., 2019; Ichinose et al., 1999; Khanh et al., 2025; Liao et al., 2017; A. C. Varquez et al., 2018), stronger solar radiation during warmer months generally tends to suppress the effect of future urbanization, as more clearly illustrated in Figure S6 and S8 in Supporting Information S1.

Tokyo's projected population reduction, which translates to the stagnation of growth in urban form and reduction in AHE, resulted in decreased projections of UTCI and $T2$ (Figures S6 and S8 in Supporting Information S1). The highest reduction was found in the winter season when background temperatures (i.e., mean monthly temperatures) and solar radiation are at their lowest levels throughout the year. With the mechanisms to be discussed in Section 3.4, $T2$ shows a greater reduction than UTCI.

In contrast, Cairo, projected to experience rapid urban growth and rising energy consumption (i.e., increasing AHE, Figure 1), shows increases in UTCI and $T2$ across nearly all months, with peak warming in January and February. Here, a negative correlation between background temperature (as shown in Figure S8 in Supporting Information S1) and projected urbanization-induced warming was found with a mechanism similar to that of Tokyo.

Meanwhile, Jakarta's tropical climate background temperatures remain within a narrow range throughout the year. Furthermore, Jakarta showed future urbanization-induced warming of similar magnitude to Cairo when compared over overlapping background temperature ranges (Figure S8 in Supporting Information S1), but without the obvious negative correlation. Focusing on the same range of background temperature (Figure S9 in Supporting Information S1), Jakarta shows a wider variability than Cairo. Influenced by background climate, the higher precipitation amount, which translates to higher inter-scenario variability, in Jakarta (Figure S10 in Supporting Information S1), is a primary reason for this. Well considered in the WRF model, the presence of large-scale clouds and rainfall non-linearly altered the surface energy balance, influencing not only $T2$ but also other meteorological variables, such as radiation and winds, that are used to calculate UTCI (Oke et al., 2017).

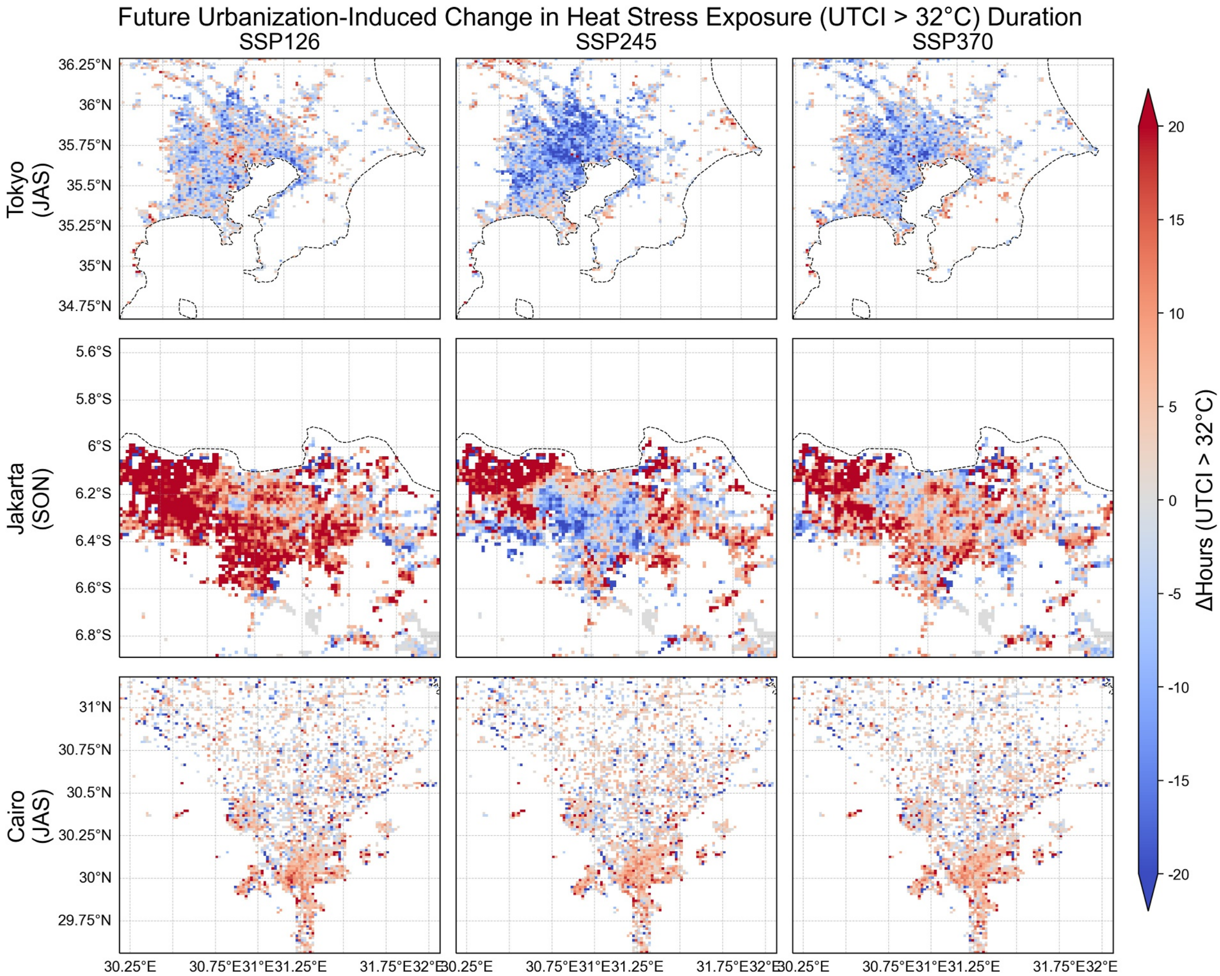

Figure 3. Spatial distribution of the urbanization-induced change in the duration of strong heat-stress exposure (UTCI $>$ 32°C; $\Delta UP = FU - PU$). Rows show Tokyo (JAS), Jakarta (SON), and Cairo (JAS), and columns show SSP126, SSP245, and SSP370. Colors indicate the grid-cell-level change in the number of hours with UTCI $>$ 32°C attributable to projected future urbanization under the same future climate forcing; positive values indicate increased strong heat-stress exposure duration and negative values indicate reduced strong heat-stress exposure duration.

3.3. Spatial Patterns of Urbanization-Induced Changes in Strong Heat-Stress Exposure

Figure 3 shows the spatial distribution of changes in strong heat-stress exposure induced by projected urbanization, expressed as changes in the number of hours with UTCI > 32 °C at each urban grid cell during the warm period of the year for each city. Table 1 summarizes the corresponding city-scale exceedance counts and baseline-normalized changes by aggregating exceedance hours over urban grid cells in each simulation. Here, one urban grid-cell hour refers to one urban grid cell at one hourly model output time step; thus, $N_{case}^{>32}$ denotes the cumulative number of urban grid-cell hours with UTCI > 32 °C in simulation *case*, where $case \in \{\mathrm{P}, \mathrm{PU}, \mathrm{FU}\}$. This count integrates both the spatial extent and temporal duration of strong heat-stress exposure. Percentage changes are expressed relative to $N_{P}^{>32}$, the present-day baseline exceedance count (see Text S7 in Supporting Information S1 for details).

The results show that, at the aggregate scale, urbanization-induced changes in strong heat-stress exposure vary among cities. Tokyo exhibits a near-neutral to weakly negative response (−4.46% to 0.62%), whereas Cairo and Jakarta show consistently positive urbanization contributions of 12.48%–13.85% and 8.73%–14.97%, respectively. Consequently, future urbanization slightly attenuates the background climate-change-induced increase in strong heat-stress exposure in Tokyo but amplifies it in Cairo and Jakarta. This amplification raises the total normalized increase from 17.47%–28.19% under climate forcing alone to 29.96%–42.05% in Cairo and from 18.55%–43.46% to 27.59%–54.86% in Jakarta; in contrast, the total normalized increase in Tokyo is reduced

Table 1
Monthly Exceedance Counts and Baseline-Normalized Changes in Strong Heat-Stress Exposure

City	Month	$N_P^{>32}$ (grid count)	Scenario	$N_{PU}^{>32}$	$N_{FU}^{>32}$	$N_{FU}^{>32} - N_{PU}^{>32}$	ΔE_{cli} (%)	ΔE_{tot} (%)	ΔE_{urb} (%)
TYO	7	234,849	SSP126	346,198	347,646	1,448	47.41	48.03	0.62
			SSP245	371,570	366,740	−4,830	58.22	56.16	−2.06
			SSP370	378,636	373,758	−4,878	61.23	59.15	−2.08
	8	372,418	SSP126	525,622	520,941	−4,681	41.14	39.88	−1.26
			SSP245	567,021	559,029	−7,992	52.25	50.11	−2.15
			SSP370	589,364	588,743	−621	58.25	58.09	−0.17
	9	79,369	SSP126	143,922	141,254	−2,668	81.33	77.97	−3.36
			SSP245	146,280	142,739	−3,541	84.30	79.84	−4.46
			SSP370	151,728	148,801	−2,927	91.17	87.48	−3.69
CAI	7	670,481	SSP126	787,622	871,326	83,704	17.47	29.96	12.48
			SSP245	798,729	883,985	85,256	19.13	31.84	12.72
			SSP370	810,203	896,901	86,698	20.84	33.77	12.93
	8	697,742	SSP126	823,873	911,649	87,776	18.08	30.66	12.58
			SSP245	833,128	922,541	89,413	19.40	32.22	12.81
			SSP370	853,999	944,953	90,954	22.39	35.43	13.04
	9	528,864	SSP126	642,366	711,755	69,389	21.46	34.58	13.12
			SSP245	659,294	729,885	70,591	24.66	38.01	13.35
			SSP370	677,969	751,227	73,258	28.19	42.05	13.85
JKT	9	535,684	SSP126	516,149	555,485	39,336	18.55	27.59	9.03
			SSP245	562,338	603,578	41,240	29.16	38.63	9.47
			SSP370	580,993	620,668	39,675	33.45	42.56	9.11
	10	358,982	SSP126	443,931	486,863	42,932	23.66	35.62	11.96
			SSP245	504,362	535,684	31,322	40.50	49.22	8.73
			SSP370	514,978	555,906	40,928	43.46	54.86	11.40
	11	279,637	SSP126	359,652	401,500	41,848	28.61	43.58	14.97
			SSP245	360,838	390,293	29,455	29.04	39.57	10.53
			SSP370	382,532	410,038	27,506	36.80	46.63	9.84

Note. $N_{\mathrm{case}}^{>32}$ denotes the cumulative number of urban grid-cell hours with UTCI > 32°C for a given simulation case, as defined in Section 2.2. ΔE_{cli}, ΔE_{tot}, and ΔE_{urb} denote the background climate-change effect, the combined climate-change-and-urbanization effect, and the urbanization-induced contribution, respectively. Percentage changes are normalized by $N_{\mathrm{P}}^{>32}$; detailed formulas are provided in Text S7 in Supporting Information S1.

slightly from 41.14%–91.17% to 39.88%–87.48% when future urbanization, which includes changes in land cover, urban morphology, and AHE, is considered.

Consistent with the city-scale urbanization-induced strong heat-stress exposure changes (ΔE_{urb}, in Table 1), the spatial patterns in Figure 3 show that these responses arise from distinct intra-urban structures. In Tokyo, negative anomalies prevail across much of the urban area, particularly under SSP245. When interpreted together with Figure 1b and Figure S3 in Supporting Information S1, projected urbanization in Tokyo involves only minor changes in urban parameters at the 1.5 km grid scale across most of the metropolitan area, whereas AHE decreases across most urban grid cells. The urbanization-induced reduction in the duration of strong heat-stress exposure is therefore more plausibly attributed to declining AHE than to projected horizontal/vertical urban expansion. In Cairo, positive anomalies are concentrated in the denser urban core and coincide with localized increases in urban parameters and AHE, suggesting that combined structural and energetic intensification enhances strong heat-stress exposure in already urbanized areas. Jakarta exhibits the broadest positive anomalies, especially across the western and southern sectors, and these align more closely with increases in urban parameters than with AHE. Although changes in AHE also contribute, the overall response in Jakarta appears to be driven primarily by grid-scale horizontal/vertical urban expansion. Because ΔUP includes changes within pre-existing urban areas as well as contributions from newly urbanized grid cells, these results indicate that increases in strong heat-stress exposure are concentrated mainly in rapidly developing parts of the urban domain.

This interpretation is consistent with previous urban climate research, particularly regarding the impacts of urbanization on air temperature. For Tokyo, AHE has long been recognized as a major contributor to the urban thermal environment: Ichinose et al. (1999) documented anthropogenic heat fluxes exceeding 400 W m^{-2} in central Tokyo; Ohashi et al. (2007) showed that summer urban air temperature in Tokyo is closely linked to building energy consumption and that air-conditioning waste heat intensifies weekday heat-island conditions; and Takane et al. (2022) estimated that pandemic-related reductions in central Tokyo lowered AHE markedly and reduced daytime air temperature by about 0.2°C in office districts. Adachi et al. (2012) further showed that future summertime warming in Tokyo is dominated by background climate change, with urbanization acting as a secondary modifier. Taken together, these studies support the interpretation that Tokyo's urbanization-induced reduction in strong heat-stress exposure reflects reduced AHE rather than substantial morphological change, and that this offset remains modest relative to the much larger background climate-change-induced increases in strong heat-stress exposure.

For Cairo and Jakarta, the urbanization-induced increase in strong heat-stress exposure is also consistent with previous studies. In hot-arid Egyptian cities, outdoor thermal conditions are sensitive to urban form and shading conditions (Galal et al., 2020). More generally, denser and more volumetrically developed urban form tends to intensify urban heat and can modify not only the city-mean thermal environment but also its spatial distribution (Y. Li et al., 2020). For Greater Jakarta, previous projections indicate that local urban effects are spatially heterogeneous and depend strongly on projected urban form and anthropogenic heating (Darmanto et al., 2019), while observations show that the Jakarta metropolitan area already experiences substantial urban heat island intensity (Siswanto et al., 2023). These studies support the interpretation that the urbanization-induced increase in strong heat-stress exposure in Cairo and Jakarta is physically plausible, although the dominant drivers differ between the two cities. In Cairo, the positive signal is concentrated over the urban core and is consistent with localized increases in both urban parameters and AHE. In Jakarta, the broader positive signal corresponds more closely to increases in urban parameters, suggesting that horizontal/vertical urban expansion plays the primary role, with AHE acting as an additional amplifier.

3.3.1. Monthly Exceedance Counts and Baseline-Normalized Changes in Strong Heat-Stress Exposure

$N^{>32}_{\mathrm{case}}$ denotes the cumulative number of urban grid-cell hours with UTCI > 32 °C for a given simulation case, where the case is P, PU, or FU. ΔE_{cli}, ΔE_{tot}, and ΔE_{urb} denote the background climate-change effect, the combined climate-change-and-urbanization effect, and the urbanization-induced contribution, respectively.Percentage changes are normalized by $N^{>32}_{\mathrm{P}}$; detailed formulas are provided in Text S7 in Supporting Information S1.

3.4. Drivers and Implications of Differing UTCI and T2 Responses to Projected Urbanization

Across all cities and scenarios, projected urbanization-induced changes in the monthly mean UTCI and $T2$, denoted by $\Delta UTCI(\Delta \mathrm{UP})$ and $\Delta T2(\Delta \mathrm{UP})$, respectively, are not of equal intensity (i.e., points depart from the 1:1 line in Figure 4). For Jakarta, most points cluster around the 1:1 line, indicating comparable changes in UTCI and $T2$ under future urbanization. Notable outliers occur during months of relatively high rainfall, such as in November and December in Jakarta for the SSP370 scenario (Figure 4). During these months, future urbanization resulted in contrasting effects on $T2$ and UTCI, where monthly mean $T2$ increased (decreased), but monthly mean UTCI decreased (increased) in November (December). For Cairo, most points lie above the 1:1 line, indicating a consistently greater increase in UTCI than in $T2$ under future urbanization. An exception occurs in October under SSP126, a high-rainfall month, when urbanization decreases air temperature but increases UTCI. For Tokyo, most points fall above the 1:1 line, indicating that projected urbanization-induced UTCI decreases are generally smaller than corresponding air temperature decreases. SSP370 responses are more tightly clustered, while SSP126 and SSP245 exhibit greater spread, reflecting scenario-dependent variability in background climate modulation.

To elucidate the drivers behind these discrepancies and quantify the relative contribution of future urbanization-induced changes in the meteorological drivers to the changes in the UTCI, LightGBM modeling (Section 2.4) was used to estimate feature importance. The models were trained using grid-cell-level monthly mean data over areas classified as urban under the present-day urban configuration. Each sample corresponds to a grid cell–month

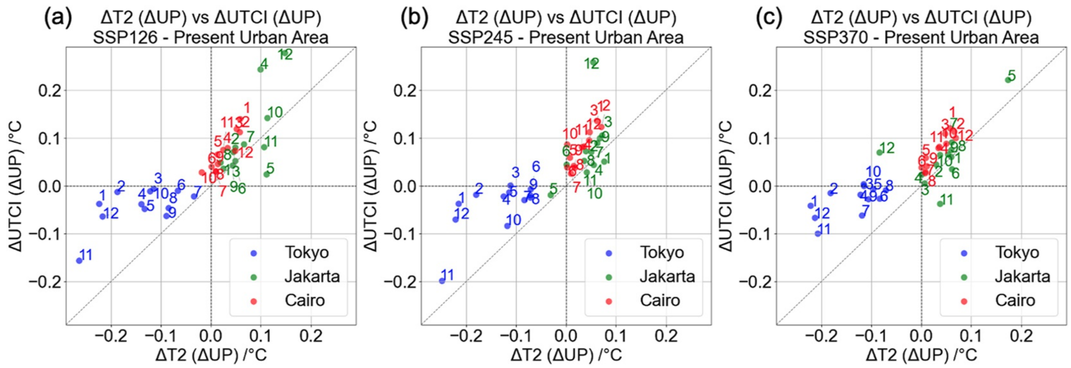

Figure 4. Comparison of future urbanization-induced T2 and Universal Thermal Climate Index changes under multiple scenarios: $\Delta T2$ (ΔUP) versus $\Delta UTCI$ (ΔUP). Red, blue, and green dots represent Cairo, Tokyo, and Jakarta, respectively. All values are spatially averaged monthly means, calculated for each month of the year, based on urban areas classified in 2022.

combination within a given city–season–scenario case (8,397 samples for Tokyo, 9,297 for Cairo, and 17,130 for Jakarta; see Text S4 in Supporting Information S1 for details). Separate models were trained independently for each city–season–scenario combination to account for regional and seasonal heterogeneity. The test-set R^2 ranged from 0.792 to 0.984 (median = 0.954). At the pixel level, MAE and RMSE for monthly mean ΔUTCI ranged from 0.0087°C to 0.0141°C and from 0.0158°C to 0.0305°C, respectively (Table S5 in Supporting Information S1). Because R^2 is sensitive to the variance of the response variable, these uniformly small absolute errors suggest that the models reproduced monthly mean ΔUTCI with high accuracy, even in cases with comparatively lower R^2. The trained models therefore provide a reasonable basis for examining model-derived feature importance within the modeling framework. Here, feature importance is used to characterize the relative contribution of meteorological predictors and their changes to model-predicted ΔUTCI associated with ΔUP, rather than to imply causal effects.

3.4.1. Factors Influencing the Differences in the Response of UTCI and $T2$ to Projected Urbanization

Figure 5 summarizes the LightGBM feature-importance analysis for the modeled ΔUTCI(ΔUP). Here, UP denotes the set of urban-related parameters that differ between the present-day and projected 2050s urban configurations, including urban land cover, urban morphology, and AHE. For brevity, $\Delta X(\Delta \mathrm{UP})$ denotes the change in meteorological variable X associated with the projected-urbanization effect, where $\Delta \mathrm{UP} = FU - PU$, whereas $\Delta X(PU - P)$ denotes the change in X associated with the future-climate background under fixed present-day urban conditions, that is, $PU - P$. Because a separate LightGBM model was trained for each city–season subset, feature importance was interpreted only within each panel, and absolute importance values were not compared across panels.

In all panels, the four predictors describing projected-urbanization-induced meteorological changes, namely $\Delta T2(\Delta \mathrm{UP})$, $\Delta T_{mrt}(\Delta \mathrm{UP})$, $\Delta RH2(\Delta \mathrm{UP})$, and $\Delta U10(\Delta \mathrm{UP})$, together accounted for 84.4%–99.8% of total feature importance, whereas the four predictors based on the $PU - P$ differences—$\Delta T2(PU - P)$, $\Delta T_{mrt}(PU - P)$, $\Delta RH2(PU - P)$, and $\Delta U10(PU - P)$—jointly explained only 0.2%–15.6%. This suggests that, within the modeling framework, the simulated response of ΔUTCI(ΔUP) depended mainly on meteorological perturbations induced by projected urban-parameter change, while the "$PU - P$" terms acted primarily as lower-importance descriptors of the background future-climate state.

Tokyo displayed the greatest within-season variation in the leading predictor. $\Delta U10(\Delta \mathrm{UP})$ ranked highest in spring and winter among all SSPs, whereas summer and autumn showed more mixed contributions from $\Delta U10(\Delta \mathrm{UP})$, $\Delta T2(\Delta \mathrm{UP})$, and $\Delta T_{mrt}(\Delta \mathrm{UP})$. In Cairo, $\Delta T2(\Delta \mathrm{UP})$ ranked highest in spring, summer, and autumn under all SSPs, while $\Delta U10(\Delta \mathrm{UP})$ ranked highest in winter; however, $\Delta RH2(\Delta \mathrm{UP})$ also made a substantial secondary contribution in several Cairo panels. In Jakarta, $\Delta U10(\Delta \mathrm{UP})$ ranked highest across all SSPs in the dry season, and under SSP126 and SSP245 in the wet season, whereas $\Delta T2(\Delta \mathrm{UP})$ slightly exceeded $\Delta U10(\Delta \mathrm{UP})$ under SSP370 in the wet season. In seven out of ten city–season panels, the highest-ranked predictor remained the

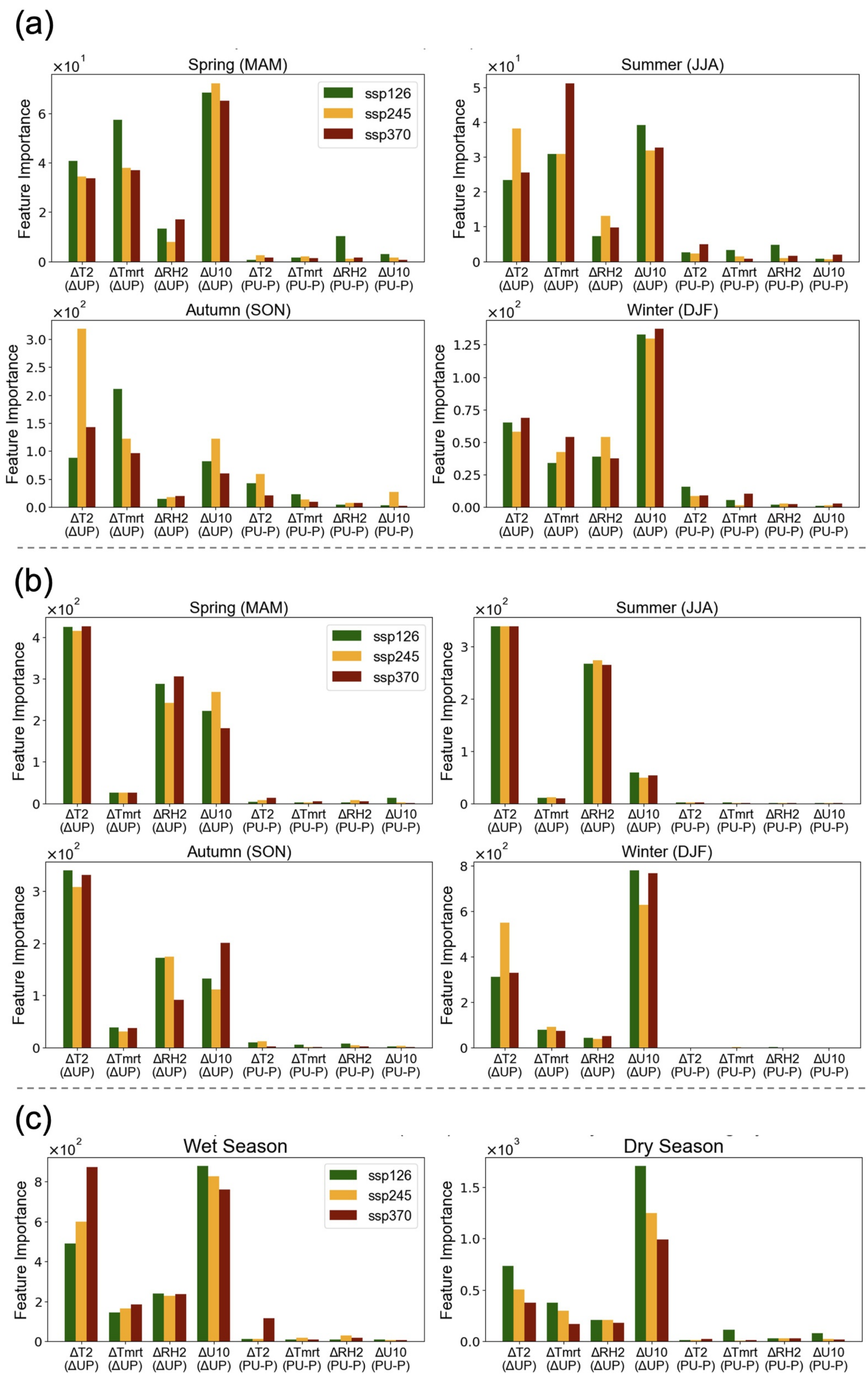

Figure 5. Feature importance of meteorological predictors for future urbanization-induced Universal Thermal Climate Index changes in (a) Tokyo, (b) Cairo, and (c) Jakarta across multiple scenarios.

same across SSPs, suggesting that the relative importance of key drivers is largely insensitive to differences in climate forcing.

These results show that the response of UTCI to projected urbanization cannot be inferred from near-surface air temperature alone. In several city–season models, especially in Tokyo and Jakarta, projected-urbanization-induced changes in wind speed and, in some panels, T_{mrt} contributed as much as or more than projected-urbanization-induced changes in near-surface air temperature. This is physically plausible because UTCI integrates the combined effects of air temperature, humidity, wind speed, and radiation rather than relying on air temperature alone (Bröde et al., 2012, 2013).

3.4.2. Implications of Differing UTCI and T2 Responses for Heat-Risk Assessment

The feature-importance patterns provide a mechanistic explanation of the differing responses of UTCI and T2 to projected urbanization. Projected urbanization can affect human thermal stress through at least three coupled pathways. First, it can alter urban surface energy partitioning and near-surface moisture availability by reducing evapotranspiration and latent heat exchange while enhancing sensible heat exchange, thereby modifying T2 and, in some cases, RH2. Second, it can modify the radiative exchange conditions through parameterized changes in urban form, thereby affecting T_{mrt}. Third, it can modify local ventilation and wind conditions through changes in aerodynamic roughness and drag, thereby affecting U10. Since UTCI reflects the combined influences of air temperature, humidity, wind, and radiant load on human heat balance, the thermal-stress response to projected urbanization depends on the relative importance of these pathways rather than on T2 alone (Bröde et al., 2012, 2013, H. Chen et al., 2022; Hao et al., 2023; Kántor & Unger, 2011).

The relatively small importance of the $PU - P$ terms does not imply that background climate is irrelevant. Rather, it suggests that, within each city–season model, the incremental urbanization signal is represented mainly by the urbanization-induced perturbation terms, while the prevailing seasonal climate modulates how strongly UTCI responds to perturbations in T2, T_{mrt}, RH2, and U10. This framework helps explain why feature importance differed among cities and variables. In Cairo, where $\Delta T2(\Delta \mathrm{UP})$ ranked first in most spring–autumn models, projected urbanization appears to be expressed mainly through a relatively direct near-surface warming pathway, which is physically consistent with enhanced sensible heating under hot and dry conditions. In Tokyo, the warm-season prominence of $\Delta T_{mrt}(\Delta \mathrm{UP})$ in several panels is also plausible, as radiative loading and T_{mrt} are known to be particularly important for outdoor thermal comfort under warm, exposed conditions. In Jakarta, by contrast, the repeated prominence of $\Delta U10(\Delta \mathrm{UP})$ indicates that ventilation changes are a key pathway through which projected urbanization modifies thermal stress in a warm-humid coastal environment, where lack of air movement itself can strongly exacerbate heat discomfort (Baruti et al., 2019; Bröde et al., 2013; Galal et al., 2020; Kántor & Unger, 2011; Zhou et al., 2023).

Figure 6 provides a spatial illustration of this mechanism in Jakarta under SSP370. In November, parts of central and eastern Jakarta show positive $\Delta U10(\Delta \mathrm{UP})$ together with negative $\Delta UTCI(\Delta \mathrm{UP})$, even where $\Delta T2(\Delta \mathrm{UP})$ is weakly positive or close to zero, suggesting that enhanced ventilation offsets part of the urbanization-induced warming signal. In December, by contrast, $\Delta U10(\Delta \mathrm{UP})$ becomes negative over much of the domain, while $\Delta UTCI(\Delta \mathrm{UP})$ becomes positive in many of the same areas despite generally weakly negative $\Delta T2(\Delta \mathrm{UP})$. A physically plausible interpretation is that projected urbanization modifies near-surface wind through competing aerodynamic and thermal effects: increased roughness and building drag tend to reduce mean near-surface wind speed, whereas urban heating can destabilize the lower atmosphere, enhance turbulent momentum exchange, and locally increase canopy-layer wind. In coastal Jakarta, the balance between these mechanisms is likely further conditioned by seasonal changes in sea-breeze behavior and the larger-scale monsoonal background flow. The November–December sign reversal of $\Delta U10$ is therefore physically plausible, but should be interpreted as a model-based inference unless supported by additional diagnostics of wind direction, pressure gradients, boundary-layer stability, or sea-breeze timing (Cheng et al., 2023; Hadi et al., 2002; Junnaedhi et al., 2023; Qiao et al., 2023; Sun et al., 2024).

The strong seasonal variability in Cairo can be interpreted within the same framework. Under the hotter spring-to-autumn background, stronger sensible heating and radiative exposure likely amplify the role of $\Delta T2(\Delta \mathrm{UP})$ in shaping ΔUTCI(ΔUP), whereas in winter, when the background thermal load is reduced, ventilation-related changes become relatively more influential. This interpretation is consistent with previous studies showing that urban form in hot-arid environments strongly affects radiation, air temperature, and wind exposure, and with

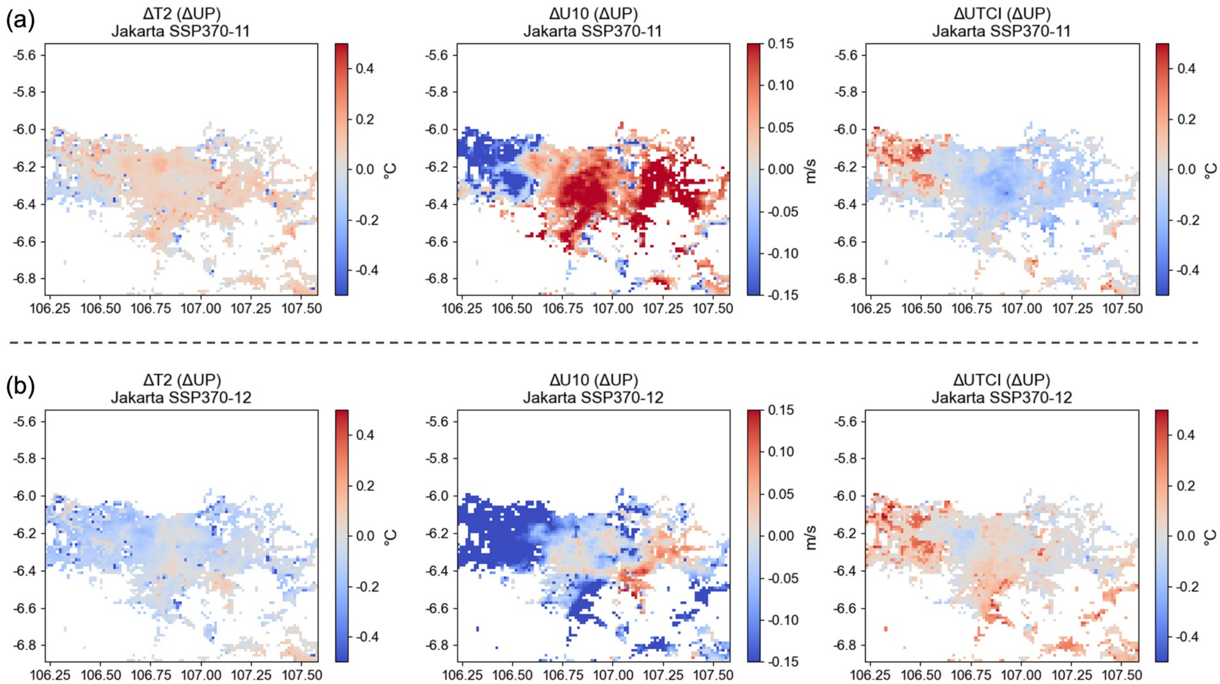

Figure 6. Spatial distributions of monthly mean $\Delta T2(\Delta UP)$, $\Delta UTCI(\Delta UP)$, and $\Delta U10(\Delta UP)$ in Jakarta for the 2050s under SSP370. These variables show projected urbanization-induced changes, calculated as the differences between two 2050s simulations under SSP370: one using the projected 2050s urban configuration and the other using the 2022 urban configuration. Panels show (a) November and (b) December.

UTCI sensitivity analyses showing greater sensitivity to humidity and radiation in hot conditions and greater sensitivity to wind when conditions are cooler (Bröde et al., 2013; Galal et al., 2020).

At the same time, the limited SSP-to-SSP reordering of the highest-ranked predictors suggests that the relative importance of key drivers remains broadly consistent across scenarios and should not be overinterpreted. In most city–season panels, the leading predictor was stable across SSPs, and where ranks changed, the leading predictors often had comparable importance. Feature importance in gradient-boosted tree models is a model-derived ranking based on split-wise loss reduction accumulated during tree construction, and correlated predictors can redistribute importance among one another when they carry overlapping predictive information. Accordingly, modest SSP-dependent changes in rank are better interpreted as differences in relative model emphasis rather than as definitive evidence of distinct scenario-specific physical regimes (Adler & Painsky, 2022; Ke et al., 2017; Strobl et al., 2007).

Finally, the analysis is based on a single simulated year, which limits generalization. One-year samples only one realization of synoptic forcing, cloudiness, humidity, and circulation variability (Brogli et al., 2023). This limitation applies to all three cities, but it is especially relevant to Jakarta and the broader Maritime Continent, where rainfall and associated circulation vary on seasonal, intraseasonal, and interannual timescales and are influenced by monsoonal flow, local air–sea interaction, and large-scale modes such as ENSO and the Indian Ocean Dipole. The present results should therefore be interpreted as process-revealing patterns for the analyzed year, while multi-year or ensemble simulations would be needed to test the robustness of the monthly wind responses and feature-importance rankings (Hendon, 2003; Lestari et al., 2019; Yamanaka, 2016).

3.5. Study Limitations and Future Perspectives

The present framework was designed for strategic city-scale assessment (Maragno et al., 2020) rather than street-level diagnosis of pedestrian thermal comfort. Although UTCI was calculated hourly before aggregation, the simulated Tmrt, wind speed, and UTCI inherit the scale mismatch of mesoscale thermal-comfort modeling (Lobaccaro et al., 2021; Martilli, Nazarian, Krayenhoff, et al., 2024). At 1.5-km resolution, shading, street-canyon geometry, vegetation, orientation-dependent radiation exposure, and flow obstruction or channeling are represented only indirectly through grid-cell urban parameters. Therefore, the results should be interpreted primarily as mesoscale indicators of relative thermal-stress change rather than as microclimatic conditions at specific pedestrian locations (Briegel et al., 2024; Ding et al., 2024; T. Jiang et al., 2023; Lobaccaro et al., 2021). This caveat is reinforced by the standard UTCI wind convention based on 10-m wind speed, which may not adequately represent wind conditions within the urban canopy layer (H. Lee et al., 2025).

Recent studies have begun to reduce this scale gap in mesoscale models through subgrid parameterizations derived from mesoscale–microclimate coupling frameworks, which may involve machine-learning-based downscaling and emulation (Briegel et al., 2024; Ding et al., 2024; T. Jiang et al., 2023; Martilli, Nazarian, Krayenhoff, et al., 2024). Among these, WRF-Comfort is particularly relevant because it estimates subgrid variability in pedestrian-level mean radiant temperature and wind speed within WRF with the BEP-BEM multi-layer urban canopy scheme, thereby supporting heat-stress diagnostics across urban areas over extended periods (Martilli, Nazarian, Krayenhoff, et al., 2024). This provides a promising pathway for improving pedestrian-level thermal-comfort diagnostics while remaining within a mesoscale modeling context. In this study, WRF-SLUCM was adopted because the available present and future urban data sets are directly compatible with grid-cell urban parameters, including land-cover change, urban morphology, and AHE, enabling computationally feasible multi-city future simulations (Khanh et al., 2021; A. C. Varquez et al., 2021). Future work could either adapt WRF-Comfort-like thermal-comfort diagnostics with the SLUCM framework or develop spatially heterogeneous SSP-consistent urbanization scenarios for more complex schemes such as BEP-BEM (Anders & Maronga, 2025; G. Chen et al., 2021; Q. Zhao et al., 2025).

A second limitation is temporal aggregation. Monthly mean UTCI provides a compact basis for comparing cities and scenarios, but it can mask whether exposure changes arise from stronger daytime radiant loading, greater evening heat persistence, or reduced nighttime cooling (Anders et al., 2025; Bröde et al., 2012; Mathew et al., 2018; Y. Qin et al., 2023). These pathways are not thermophysiologically equivalent, because hot nights can suppress nocturnal recovery and increase health risks (Di Napoli et al., 2019; Guo et al., 2024; Obradovich et al., 2017; Royé et al., 2025). The hourly threshold-exceedance analysis partly addresses this limitation by retaining hazardous hours before aggregation, but future work should explicitly separate daytime, evening, and nighttime UTCI responses and quantify the timing, persistence, and intensity of heat exposure across the diurnal cycle (Sadeghi et al., 2021).

Finally, the projections are conditional on one simulated meteorological year and one future urbanization pathway. Alternative synoptic years could modify the simulated cloudiness, humidity, circulation, and wind responses (Brogli et al., 2023), while alternative urban expansion patterns, development intensities, morphology trajectories, and AHE assumptions could modify the magnitude and spatial distribution of future UTCI changes (G. Chen et al., 2020; W. He et al., 2023; L. Jiang & O'Neill, 2017; Q. Zhao et al., 2025). Future studies should therefore use multi-year or ensemble simulations together with scenario-consistent urbanization pathways to evaluate uncertainty in climate forcing, urban extent, morphology, and AHE more systematically (Booker et al., 2025; Darmanto et al., 2019).

4. Conclusion

This study projected 1.5-km future urban climate and thermal comfort for Tokyo, Cairo, and Jakarta in the 2050s under SSP126, SSP245, and SSP370, explicitly accounting for projected changes in urban morphology and AHE. Across all cities and scenarios, both near-surface air temperature (T2) and UTCI increase, with UTCI increasing more strongly. Thus, air temperature alone would underestimate future urban heat risk. Climate forcing remains the dominant driver of city-scale mean warming, while projected urbanization mainly modulates intra-urban heterogeneity, producing local hotspots in Cairo and Jakarta whose magnitude can approach the climate-forcing signal.

Projected seasonal changes in monthly mean T2 and UTCI differ systematically with climatic background. Cairo's hot-desert setting produces the strongest summer amplification, Tokyo's humid-subtropical setting produces a moderate, partly bimodal response, and Jakarta's tropical-monsoon setting shows weak seasonality. The effects of projected urban-configuration changes on monthly mean thermal conditions also differ across cities. In Tokyo, this specific future urban pathway slightly reduces monthly mean T2 and UTCI relative to the climate-only simulations, mainly because urban morphology changes only slightly while AHE declines. In contrast, projected horizontal/vertical urban expansion, together with rising AHE, further increases monthly mean thermal stress in Cairo and Jakarta.

The threshold-exceedance analysis provides a clear heat-risk message. Averaged across the analyzed warm months and SSPs, total baseline-normalized exposure to strong heat stress, defined as hours with UTCI > 32°C, increases by 61.9% in Tokyo, 34.3% in Cairo, and 42.0% in Jakarta. Projected urbanization contributes differently to these increases: it is near-neutral to negative in Tokyo due to declining AHE, with an average contribution of −2.1 percentage points and a range of −4.46% to +0.62%, but substantially amplifies exposure in Cairo and Jakarta, with average contributions of +13.0 and +10.6 percentage points, respectively. These positive contributions are consistent across scenarios in Cairo (+12.48% to +13.85%) and Jakarta (+8.73% to +14.97%), showing that urbanization materially modifies hazardous thermal-stress exposure.

These results have direct implications for urban heat adaptation. The Tokyo case suggests that reducing AHE can partly counteract background climate-change-induced increases in strong UTCI exposure, although the offset remains modest relative to the larger background climate signal. Conversely, Cairo and Jakarta show that projected horizontal/vertical urban expansion and increasing AHE can amplify future heat-stress exposure. Finally, the UTCI response to projected urbanization cannot be inferred from T2 alone: air temperature, radiation, humidity, and wind play different roles by city and season, with ventilation changes especially important in Jakarta. These findings emphasize the need to assess future urban heat risk using physiologically relevant indices such as UTCI, together with explicit representation of urban morphology and AHE.

Conflict of Interest

The authors declare no conflicts of interest relevant to this study.

Availability Statement

The NCEP GDAS/FNL 0.25° Global Tropospheric Analyses and Forecast Grids used as meteorological initial and lateral boundary conditions in this study are available from the NSF National Center for Atmospheric Research (National Centers for Environmental Prediction, National Weather Service, NOAA, U.S. Department of Commerce, 2015). The CMIP6 ScenarioMIP outputs used to construct the PGW perturbations were obtained from the Earth System Grid Federation. Twenty-six candidate CMIP6 source IDs were initially considered, and the final PGW ensemble was constructed from the subset of models with complete monthly data for the required variables, SSP scenarios, native-grid data and analysis periods. The IDs of the sources selected, the models retained, the availability of the SSP and the corresponding formal citations of the CMIP6 dataset are listed in Table S2 in Supporting Information S1 (Danabasoglu, 2019; Dix et al., 2019; W. L. Lee & Liang, 2020; Lovato & Peano, 2020; NASA Goddard Institute for Space Studies (NASA/GISS), 2020a, 2020b; Schupfner et al., 2019, 2021; Seland et al., 2019; Semmler et al., 2019; Shiogama et al., 2019; Swart et al., 2019a, 2019b; Yukimoto et al., 2019; Ziehn et al., 2019). Version 4.6.0 of the WRF Model used in this study is available from the WRF Model development team (WRF Model Development Team, 2024). The global 1-km present and future hourly anthropogenic heat flux data set is available from Varquez et al. (A. C. G. Varquez, Kiyomoto, et al., 2020). The present and future 1-km resolution global population density and urban morphological parameters dataset is available from Khanh et al. (2021). UTCI was calculated using the operational UTCI procedure (Bröde et al., 2012) and the UTCI Calculator (COST Action 730 and ISB Commission 6, 2025). All third-party data and software cited above are publicly available.

Acknowledgments
This work was supported by JSPS KAKENHI (Grants JP23K28289 and JP25K00040) and JST SPRING (Grant JPMJSP2180).

References

Adachi, S. A., Kimura, F., Kusaka, H., Inoue, T., & Ueda, H. (2012). Comparison of the impact of global climate changes and urbanization on summertime future climate in the Tokyo metropolitan area. *Journal of Applied Meteorology and Climatology*, *51*(8), 1441–1454. https://doi.org/10.1175/JAMC-D-11-0137.1

Adler, A. I., & Painsky, A. (2022). Feature importance in gradient boosting trees with cross-validation feature selection. *Entropy*, *24*(5), 687. https://doi.org/10.3390/e24050687

Anders, J., & Maronga, B. (2025). Urban microscale simulations based on a local climate zone wizard: Concept and validation using the palm model system. *Urban Climate*, *63*, 102576. https://doi.org/10.1016/j.uclim.2025.102576

Anders, J., Schubert, S., Maronga, B., & Salim, M. (2025). Simplifying heat stress assessment: Evaluating meteorological variables as single indicators of outdoor thermal comfort in urban environments. *Building and Environment*, *274*, 112658. https://doi.org/10.1016/j.buildenv.2025.112658

Ao, X., Huang, W., Zhang, N., Li, J., & Sun, Y. (2024). Impact of urban canopy physics and detailed urban canopy parameters on high-resolution simulation over two large urban agglomerations in China. *Urban Climate*, *55*, 101922. https://doi.org/10.1016/j.uclim.2024.101922

Baruti, M. M., Johansson, E., & AAstrand, J. (2019). Review of studies on outdoor thermal comfort in warm humid climates: Challenges of informal urban fabric. *International Journal of Biometeorology*, *63*(10), 1449–1462. https://doi.org/10.1007/s00484-019-01757-3

Best, M. J., Abramowitz, G., Johnson, H. R., Pitman, A. J., Balsamo, G., Boone, A., et al. (2015). The plumbing of land surface models: Benchmarking model performance. *Journal of Hydrometeorology*, *16*(3), 1425–1442. https://doi.org/10.1175/JHM-D-14-0158.1

Blazejczyk, K. (1994). New climatological-and-physiological model of the human heat balance outdoor (menex) and its applications in bioclimatological studies in different scales. *Zeszyty IGiPZ PAN*, *28*, 27–58.

Blazejczyk, K., Epstein, Y., Jendritzky, G., Staiger, H., & Tinz, B. (2012). Comparison of UTCI to selected thermal indices. *International Journal of Biometeorology*, *56*(3), 515–535. https://doi.org/10.1007/s00484-011-0453-2

Blunden, J., Boyer, T., & Bartow-Gillies, E. (2023). State of the climate in 2022. *Bulletin of the American Meteorological Society*, *104*(9), S1–S501. https://doi.org/10.1175/2023BAMSStateoftheClimate.1

Booker, K., White, I., Fu, X., & Wilson, M. (2025). Modelling urban growth for long-term planning under future climate uncertainty: A systematic review and decision pathway. *Cities*, *167*, 106310. https://doi.org/10.1016/j.cities.2025.106310

Briegel, F., Schrodi, S., Sulzer, M., Brox, T., Pinto, J. G., & Christen, A. (2025). Deep learning enables city-wide climate projections of street-level heat stress. *Urban Climate*, *62*, 102564. https://doi.org/10.1016/j.uclim.2025.102564

Briegel, F., Wehrle, J., Schindler, D., & Christen, A. (2024). High-resolution multi-scaling of outdoor human thermal comfort and its intra-urban variability based on machine learning. *Geoscientific Model Development*, *17*(4), 1667–1688. https://doi.org/10.5194/gmd-17-1667-2024

Bröde, P., Blazejczyk, K., Fiala, D., Havenith, G., Holmer, I., Jendritzky, G., & Kampmann, B. (2013). The universal thermal climate index utci compared to ergonomics standards for assessing the thermal environment. *Industrial Health*, *51*(1), 16–24.

Bröde, P., Fiala, D., Błażejczyk, K., Epstein, Y., Holmér, I., Jendritzky, G., et al. (2012). Deriving the operational procedure for the universal thermal climate index (UTCI). *International Journal of Biometeorology*, *56*(3), 481–494. https://doi.org/10.1007/s00484-011-0454-1

Brogli, R., Heim, C., Mensch, J., Sørland, S. L., & Schär, C. (2023). The pseudo-global-warming (pgw) approach: Methodology, software package PGW4ERA5 v1.1, validation, and sensitivity analyses. *Geoscientific Model Development*, *16*(3), 907–926. https://doi.org/10.5194/gmd-16-907-2023

Castells-Quintana, D., Krause, M., & McDermott, T. K. J. (2021). The urbanising force of global warming: The role of climate change in the spatial distribution of population. *Journal of Economic Geography*, *21*(4), 531–556. https://doi.org/10.1093/jeg/lbaa030

Chapman, S., Watson, J. E., Salazar, A., Thatcher, M., & McAlpine, C. A. (2017). The impact of urbanization and climate change on urban temperatures: A systematic review. *Landscape Ecology*, *32*(10), 1921–1935. https://doi.org/10.1007/s10980-017-0561-4

Chen, B., Wu, C., Liu, X., Chen, L., Wu, J., Yang, H., et al. (2019). Seasonal climatic effects and feedbacks of anthropogenic heat release due to global energy consumption with CAM5. *Climate Dynamics*, *52*(11), 6377–6390. https://doi.org/10.1007/s00382-018-4528-1

Chen, F., Kusaka, H., Bornstein, R., Ching, J., Grimmond, C. S. B., Grossman-Clarke, S., et al. (2011). The integrated WRF/urban modelling system: Development, evaluation, and applications to urban environmental problems. *International Journal of Climatology*, *31*(2), 273–288. https://doi.org/10.1002/joc.2158

Chen, G., Li, X., Liu, X., Chen, Y., Liang, X., Leng, J., et al. (2020). Global projections of future urban land expansion under shared socioeconomic pathways. *Nature Communications*, *11*(1), 537. https://doi.org/10.1038/s41467-020-14386-x

Chen, G., Xie, J., Li, W., Li, X., Chung, L. C. H., Ren, C., & Liu, X. (2021). Future "local climate zone" spatial change simulation in greater bay area under the shared socioeconomic pathways and ecological control line. *Building and Environment*, *203*, 108077. https://doi.org/10.1016/j.buildenv.2021.108077

Chen, H., Huang, J. J., Dash, S. S., McBean, E., Wei, Y., & Li, H. (2022). Assessing the impact of urbanization on urban evapotranspiration and its components using a novel four-source energy balance model. *Agricultural and Forest Meteorology*, *316*, 108853. https://doi.org/10.1016/j.agrformet.2022.108853

Cheng, G., Schlünzen, K. H., Grawe, D., Voss, V., Thatcher, M., & Rayner, P. (2023). Parameterizing building effects on airflows within the urban canopy layer for high-resolution models using a nudging approach. *Quarterly Journal of the Royal Meteorological Society*, *149*(755), 2617–2633. https://doi.org/10.1002/qj.4524

COST Action 730 and ISB Commission 6. (2025). Utci calculator [Software]. *UTCI*. Retrieved from https://www.utci.org/utci_calc.php

Danabasoglu, G. (2019). Ncar CESM2 model output prepared for CMIP6 ScenarioMIP [Dataset]. *Earth System Grid Federation*. https://doi.org/10.22033/ESGF/CMIP6.2201

Darmanto, N. S., Varquez, A. C. G., Kawano, N., & Kanda, M. (2019). Future urban climate projection in a tropical megacity based on global climate change and local urbanization scenarios. *Urban Climate*, *29*, 100482. https://doi.org/10.1016/j.uclim.2019.100482

Di Napoli, C., Barnard, C., Prudhomme, C., Cloke, H. L., & Pappenberger, F. (2021). Era5-heat: A global gridded historical dataset of human thermal comfort indices from climate reanalysis. *Geoscience Data Journal*, *8*(1), 2–10. https://doi.org/10.1002/gdj3.102

Di Napoli, C., Pappenberger, F., & Cloke, H. L. (2019). Verification of heat stress thresholds for a health-based heat-wave definition. *Journal of Applied Meteorology and Climatology*, *58*(6), 1177–1194. https://doi.org/10.1175/jamc-d-18-0246.1

Ding, X., Zhao, Y., Strebel, D., Fan, Y., Ge, J., & Carmeliet, J. (2024). A WRF-UCM-solweig framework for mapping thermal comfort and quantifying urban climate drivers: Advancing spatial and temporal resolutions at city scale. *Sustainable Cities and Society*, *112*, 105628. https://doi.org/10.1016/j.scs.2024.105628

Dix, M., Bi, D., Dobrohotoff, P., Fiedler, R., Harman, I., Law, R., et al. (2019). CSIRO-arccss access-CM2 model output prepared for CMIP6 ScenarioMIP [Dataset]. *Earth System Grid Federation*. https://doi.org/10.22033/ESGF/CMIP6.2285

Endo, T., Minami, S., Nomura, A., Ohtsuji, H., Kato, J., Miwa, M., & Sakamoto, R. (2023). Challenges in computing resource sharing towards next-gen interactive accelerated HPC. In *International conference on high performance computing* (pp. 231–242). Springer Nature Switzerland.

Epstein, Y., & Moran, D. S. (2006). Thermal comfort and the heat stress indices. *Industrial Health*, *44*(3), 388–398. https://doi.org/10.2486/indhealth.44.388

Eyring, V., Bony, S., Meehl, G. A., Senior, C. A., Stevens, B., Stouffer, R. J., & Taylor, K. E. (2016). Overview of the coupled model intercomparison project phase 6 (CMIP6) experimental design and organization. *Geoscientific Model Development*, *9*(5), 1937–1958. https://doi.org/10.5194/gmd-9-1937-2016

Fiala, D., Havenith, G., Bröde, P., Kampmann, B., & Jendritzky, G. (2012). UTCI-Fiala multi-node model of human heat transfer and temperature regulation. *International Journal of Biometeorology*, *56*(3), 429–441. https://doi.org/10.1007/s00484-011-0424-7

Fricko, O., Havlik, P., Rogelj, J., Klimont, Z., Gusti, M., Johnson, N., et al. (2017). The marker quantification of the shared socioeconomic pathway 2: A middle-of-the-road scenario for the 21st century. *Global Environmental Change*, *42*, 251–267. https://doi.org/10.1016/j.gloenvcha.2016.06.004

Fujimori, S., Hasegawa, T., Masui, T., Takahashi, K., Herran, D. S., Dai, H., et al. (2017). SSP3: Aim implementation of shared socioeconomic pathway. *Global Environmental Change*, *42*, 268–283. https://doi.org/10.1016/j.gloenvcha.2016.06.009

Galal, O. M., Sailor, D. J., & Mahmoud, H. (2020). The impact of urban form on outdoor thermal comfort in hot arid environments during daylight hours, case study: New Aswan. *Building and Environment*, *184*, 107222. https://doi.org/10.1016/j.buildenv.2020.107222

Gier, B. K., Schlund, M., Friedlingstein, P., Jones, C. D., Jones, C., Zaehle, S., & Eyring, V. (2024). Representation of the terrestrial carbon cycle in CMIP6. *Biogeosciences*, *21*(22), 5321–5360. https://doi.org/10.5194/bg-21-5321-2024

Giorgi, F., & Mearns, L. O. (1991). Approaches to the simulation of regional climate change: A review. *Reviews of Geophysics*, *29*(2), 191–216. https://doi.org/10.1029/90rg02636

Giridharan, R., & Emmanuel, R. (2018). The impact of urban compactness, comfort strategies and energy consumption on tropical urban heat island intensity: A review. *Sustainable Cities and Society*, *40*, 677–687. https://doi.org/10.1016/j.scs.2018.01.024

Goodess, C., Berk, S., Ratna, S. B., Brousse, O., Davies, M., Heaviside, C., et al. (2021). Climate change projections for sustainable and healthy cities. *Buildings and Cities*, *2*(1), 812–836. https://doi.org/10.5334/bc.111

Gulyás, Unger, J., & Matzarakis, A. (2006). Assessment of the microclimatic and human comfort conditions in a complex urban environment: Modelling and measurements. *Building and Environment*, *41*(12), 1713–1722. https://doi.org/10.1016/j.buildenv.2005.07.001

Guo, Y. T., Chan, K. H., Qiu, H., Wong, E. L.-Y., & Ho, K. F. (2024). The risk of hospitalization associated with hot nights and excess nighttime heat in a subtropical metropolis: A time-series study in Hong Kong, 2000–2019. *Lancet Regional Health. Western Pacific*, *51*, 101168. https://doi.org/10.1016/j.lanwpc.2024.101168

Hadi, T. W., Horinouchi, T., Tsuda, T., Hashiguchi, H., & Fukao, S. (2002). Sea-breeze circulation over Jakarta, Indonesia: A climatology based on boundary layer radar observations. *Monthly Weather Review*, *130*(9), 2153–2166. https://doi.org/10.1175/1520-0493(2002)130<2153:sbcoji>2.0.co;2

Hamdi, R., Kusaka, H., Doan, Q.-V., Cai, P., He, H., Luo, G., et al. (2020). The state-of-the-art of urban climate change modeling and observations. *Earth Systems and Environment*, *4*(4), 631–646. https://doi.org/10.1007/s41748-020-00193-3

Hao, L., Sun, G., Huang, X., Tang, R., Jin, K., Lai, Y., et al. (2023). Urbanization alters atmospheric dryness through land evapotranspiration. *npj Climate and Atmospheric Science*, *6*(1), 149. https://doi.org/10.1038/s41612-023-00479-z

Havenith, G., Fiala, D., Błazejczyk, K., Richards, M., Bröde, P., Holmér, I., et al. (2012). The UTCI-clothing model. *International Journal of Biometeorology*, *56*(3), 461–470. https://doi.org/10.1007/s00484-011-0451-4

He, W., Li, X., Zhou, Y., Shi, Z., Yu, G., Hu, T., et al. (2023). Global urban fractional changes at a 1 km resolution throughout 2100 under eight scenarios of shared socioeconomic pathways (SSPS) and representative concentration pathways (RCPS). *Earth System Science Data*, *15*(8), 3623–3639. https://doi.org/10.5194/essd-15-3623-2023

He, X., Li, Y., Wang, X., Chen, L., Yu, B., Zhang, Y., & Miao, S. (2019). High-resolution dataset of urban canopy parameters for Beijing and its application to the integrated wrf/urban modelling system. *Journal of Cleaner Production*, *208*, 373–383. https://doi.org/10.1016/j.jclepro.2018.10.086

Helbling, M., & Meierrieks, D. (2023). Global warming and urbanization. *Journal of Population Economics*, *36*(3), 1187–1223. https://doi.org/10.1007/s00148-022-00924-y

Hendon, H. H. (2003). Indonesian rainfall variability: Impacts of ENSO and local air–sea interaction. *Journal of Climate*, *16*(11), 1775–1790. https://doi.org/10.1175/1520-0442(2003)016<1775:irvioe>2.0.co;2

Hiroki, R., Varquez, A. C., Khanh, D. N., Rynazal, R., Renard, F., Alonso, L., & Kanda, M. (2025). Long-term changes of universal thermal climate index (UTCI) estimated from weather stations and gradient-boosted decision trees throughout Japan. *International Journal of Climatology*, *45*(8), e8843. https://doi.org/10.1002/joc.8843

Höppe, P. (2002). Different aspects of assessing indoor and outdoor thermal comfort. *Energy and Buildings*, *34*(6), 661–665. https://doi.org/10.1016/s0378-7788(02)00017-8

Hundhausen, M., Feldmann, H., Laube, N., & Pinto, J. G. (2023). Future heat extremes and impacts in a convection-permitting climate ensemble over Germany. *Natural Hazards and Earth System Sciences*, *23*(8), 2873–2893. https://doi.org/10.5194/nhess-23-2873-2023

Ichinose, T., Shimodozono, K., & Hanaki, K. (1999). Impact of anthropogenic heat on urban climate in Tokyo. *Atmospheric Environment*, *33*(24–25), 3897–3909. https://doi.org/10.1016/s1352-2310(99)00132-6

Inoue, T., & Matsumoto, J. (2003). Seasonal and secular variations of sunshine duration and natural seasons in Japan. *International Journal of Climatology: A Journal of the Royal Meteorological Society*, *23*(10), 1219–1234. https://doi.org/10.1002/joc.933

IPCC. (2021). Climate change 2021: The physical science basis. In V. Masson-Delmotte, P. Zhai, A. Pirani, S. L. Connors, C. Péan, S. Berger, et al. (Eds.), *Contribution of working group i to the sixth assessment report of the intergovernmental panel on climate change*. Cambridge University Press. https://doi.org/10.1017/9781009157896

Jendritzky, G., De Dear, R., & Havenith, G. (2012). UTCI—Why another thermal index? *International Journal of Biometeorology*, *56*(3), 421–428. https://doi.org/10.1007/s00484-011-0513-7

Jiang, L., & O'Neill, B. C. (2017). Global urbanization projections for the shared socioeconomic pathways. *Global Environmental Change*, *42*, 193–199. https://doi.org/10.1016/j.gloenvcha.2015.03.008

Jiang, T., Krayenhoff, E. S., Voogt, J. A., Warland, J., Demuzere, M., & Moede, C. (2023). Dynamically downscaled projection of urban outdoor thermal stress and indoor space cooling during future extreme heat. *Urban Climate*, *51*, 101648. https://doi.org/10.1016/j.uclim.2023.101648

Junnaedhi, I. D. G. A., Inagaki, A., Ferdiansyah, M. R., & Kanda, M. (2023). Seasonal sea breeze variation analysis based on multi-year near-surface observations in Jakarta, Indonesia. *International Journal of Climatology*, *43*(11), 5177–5195. https://doi.org/10.1002/joc.8139

Kanda, M., Inagaki, A., Miyamoto, T., Gryschka, M., & Raasch, S. (2013). A new aerodynamic parametrization for real urban surfaces. *Boundary-Layer Meteorology*, *148*(2), 357–377. https://doi.org/10.1007/s10546-013-9818-x

Kántor, N., & Unger, J. (2011). The most problematic variable in the course of human-biometeorological comfort assessment—The mean radiant temperature. *Open Geosciences*, *3*(1), 90–100. https://doi.org/10.2478/s13533-011-0010-x

Karlický, J., Huszár, P., Halenka, T., Belda, M., Žák, M., Pišoft, P., & Mikšovský, J. (2018). Multi-model comparison of urban heat island modelling approaches. *Atmospheric Chemistry and Physics*, *18*(14), 10655–10674. https://doi.org/10.5194/acp-18-10655-2018

Ke, G., Meng, Q., Finley, T., Wang, T., Chen, W., Ma, W., et al. (2017). Lightgbm: A highly efficient gradient boosting decision tree. In *Advances in neural information processing systems* (Vol. 30, pp. 3149–3157).

Khanh, D. N., Varquez, A. C., & Kanda, M. (2021). Present and future 1 km resolution global population density and urban morphological parameters. *Figshare*. https://doi.org/10.6084/m9.figshare.17108981

Khanh, D. N., Varquez, A. C., & Kanda, M. (2023). Impact of urbanization on exposure to extreme warming in megacities. *Heliyon*, *9*(4), e15511. https://doi.org/10.1016/j.heliyon.2023.e15511

Khanh, D. N., Varquez, A. C., & Kanda, M. (2025). Impact of anthropogenic heat on air temperature: A first-order estimate using dimensional analysis and numerical simulations. *Geophysical Research Letters*, *52*(11), e2024GL114400. https://doi.org/10.1029/2024GL114400

Kimura, F., & Kitoh, A. (2007). Downscaling by pseudo global warming method. In *The final report of ICCAP* (Vol. 4346, pp. 463–478).

Kusaka, H., Hara, M., & Takane, Y. (2012). Urban climate projection by the WRF model at 3-km horizontal grid increment: Dynamical downscaling and predicting heat stress in the 2070's August for Tokyo, Osaka, and Nagoya metropolises. *Journal of the Meteorological Society of Japanese Series II*, *90*, 47–63. https://doi.org/10.2151/jmsj.2012-B04

Kusaka, H., Kondo, H., Kikegawa, Y., & Kimura, F. (2001). A simple single-layer urban canopy model for atmospheric models: Comparison with multi-layer and slab models. *Boundary-Layer Meteorology*, *101*(3), 329–358. https://doi.org/10.1023/a:1019207923078
Lai, D., Lian, Z., Liu, W., Guo, C., Liu, W., Liu, K., & Chen, Q. (2020). A comprehensive review of thermal comfort studies in urban open spaces. *Science of the Total Environment*, *742*, 140092. https://doi.org/10.1016/j.scitotenv.2020.140092
Lankao, P. R., & Qin, H. (2011). Conceptualizing urban vulnerability to global climate and environmental change. *Current Opinion in Environmental Sustainability*, *3*(3), 142–149.
Leal Filho, W., Balogun, A.-L., Olayide, O. E., Azeiteiro, U. M., Ayal, D. Y., Muñoz, P. D. C., et al. (2019). Assessing the impacts of climate change in cities and their adaptive capacity: Towards transformative approaches to climate change adaptation and poverty reduction in urban areas in a set of developing countries. *Science of the Total Environment*, *692*, 1175–1190. https://doi.org/10.1016/j.scitotenv.2019.07.227
Lee, H., Park, S., & Mayer, H. (2025). Approach for the vertical wind speed profile implemented in the UTCI basics blocks UTCI applications at the urban pedestrian level. *International Journal of Biometeorology*, *69*(3), 567–580. https://doi.org/10.1007/s00484-024-02835-x
Lee, W.-L., & Liang, H.-C. (2020). AS-RCEC TaiESM1.0 model output prepared for CMIP6 ScenarioMIP [Dataset]. *Earth System Grid Federation*. https://doi.org/10.22033/ESGF/CMIP6.9688
Lestari, S., King, A., Vincent, C., Karoly, D., & Protat, A. (2019). Seasonal dependence of rainfall extremes in and around Jakarta, Indonesia. *Weather and Climate Extremes*, *24*, 100202. https://doi.org/10.1016/j.wace.2019.100202
Li, C., Zhou, Y., Wu, M., Xu, J., & Fu, X. (2025). Exploring nonlinear threshold effects and interactions between built environment and urban vitality at the block level using machine learning. *Land*, *14*(6), 1232. https://doi.org/10.3390/land14061232
Li, X., Stringer, L. C., & Dallimer, M. (2022). The impacts of urbanisation and climate change on the urban thermal environment in Africa. *Climate*, *10*(11), 164. https://doi.org/10.3390/cli10110164
Li, Y., Fei, W., Yang, M., Wang, Y., Du, Y., & Wang, Y. (2025). How to realize large-scale outdoor thermal comfort studies? A systematic review based on otc characterization, methods and research trends. *Frontiers in Sustainable Cities*, *7*, 1552994. https://doi.org/10.3389/frsc.2025.1552994
Li, Y., Schubert, S., Kropp, J. P., & Rybski, D. (2020). On the influence of density and morphology on the Urban Heat Island intensity. *Nature Communications*, *11*(1), 2647. https://doi.org/10.1038/s41467-020-16461-9
Liao, W., Liu, X., Wang, D., & Sheng, Y. (2017). The impact of energy consumption on the surface urban heat island in China's 32 major cities. *Remote Sensing*, *9*(3), 250. https://doi.org/10.3390/rs9030250
Liu, S., Xie, Y., Zhu, Y., Lin, B., Cao, B., Wong, N. H., et al. (2022). Comparative analysis on indoor and outdoor thermal comfort in transitional seasons and summer based on multiple databases: Lessons learnt from the outdoors. *Science of the Total Environment*, *848*, 157694. https://doi.org/10.1016/j.scitotenv.2022.157694
Liu, Y., Chen, F., Warner, T., & Basara, J. (2006). Verification of a mesoscale data-assimilation and forecasting system for the Oklahoma City area during the Joint Urban 2003 field project. *Journal of Applied Meteorology and Climatology*, *45*(7), 912–929. https://doi.org/10.1175/JAM2416.1
Lobaccaro, G., De Ridder, K., Acero, J. A., Hooyberghs, H., Lauwaet, D., Maiheu, B., et al. (2021). Applications of models and tools for mesoscale and microscale thermal analysis in mid-latitude climate regions—A review. *Sustainability*, *13*(22), 12385. https://doi.org/10.3390/su132212385
Lovato, T., & Peano, D. (2020). Cmcc CMCC-CM2-SR5 model output prepared for CMIP6 ScenarioMIP [Dataset]. *Earth System Grid Federation*. https://doi.org/10.22033/ESGF/CMIP6.1365
Macagba, S., & Delina, L. (2024). The state and future of extreme heat studies in southeast asian megacities: Risk, impacts and adaptation strategies in a warming world. *Environmental Research Communications*, *6*(11), 112003. https://doi.org/10.1088/2515-7620/ad9145
Maragno, D., Dalla Fontana, M., & Musco, F. (2020). Mapping heat stress vulnerability and risk assessment at the neighborhood scale to drive urban adaptation planning. *Sustainability*, *12*(3), 1056. https://doi.org/10.3390/su12031056
Martilli, A. (2007). Current research and future challenges in urban mesoscale modelling. *International Journal of Climatology: A Journal of the Royal Meteorological Society*, *27*(14), 1909–1918. https://doi.org/10.1002/joc.1620
Martilli, A., Clappier, A., & Rotach, M. W. (2002). An urban surface exchange parameterisation for mesoscale models. *Boundary-Layer Meteorology*, *104*(2), 261–304. https://doi.org/10.1023/a:1016099921195
Martilli, A., Nazarian, N., Krayenhoff, E. S., Lachapelle, J., Lu, J., Rivas, E., et al. (2024). Wrf-comfort: Simulating microscale variability in outdoor heat stress at the city scale with a mesoscale model. *Geoscientific Model Development*, *17*(12), 5023–5039. https://doi.org/10.5194/gmd-17-5023-2024
Masson, V., Grimmond, C. S. B., & Oke, T. R. (2002). Evaluation of the town energy balance (teb) scheme with direct measurements from dry districts in two cities. *Journal of applied meteorology*, *41*(10), 1011–1026.
Mathew, A., Khandelwal, S., Kaul, N., & Chauhan, S. (2018). Analyzing the diurnal variations of land surface temperatures for surface urban heat island studies: Is time of observation of remote sensing data important? *Sustainable Cities and Society*, *40*, 194–213. https://doi.org/10.1016/j.scs.2018.03.032
McCarthy, M. P., Best, M. J., & Betts, R. A. (2010). Climate change in cities due to global warming and urban effects. *Geophysical Research Letters*, *37*(9). https://doi.org/10.1029/2010gl042845
Moazzam, M. F. U., Doh, Y.-H., & Lee, B.-G. (2022). Impact of urbanization on land surface temperature and surface urban heat island using optical remote sensing data: A case study of Jeju Island, Republic of Korea. *Building and Environment*, *222*, 109368. https://doi.org/10.1016/j.buildenv.2022.109368
National Centers for Environmental Prediction, National Weather Service, NOAA, U.S. Department of Commerce. (2015). *NCEP GDAS/FNL 0.25 degree global tropospheric analyses and forecast grids*. NSF National Center for Atmospheric Research. https://doi.org/10.5065/D65Q4T4Z
NASA Goddard Institute for Space Studies (NASA/GISS). (2020a). NASA-GISS GISS-E2.1G model output prepared for CMIP6 ScenarioMIP [Dataset]. *Earth System Grid Federation*. https://doi.org/10.22033/ESGF/CMIP6.2074
NASA Goddard Institute for Space Studies (NASA/GISS). (2020b). NASA-GISS GISS-E2.1H model output prepared for CMIP6 ScenarioMIP [Dataset]. *Earth System Grid Federation*. https://doi.org/10.22033/ESGF/CMIP6.2080
Nazarian, N., Krayenhoff, E. S., Bechtel, B., Hondula, D. M., Paolini, R., Vanos, J., et al. (2022). Integrated assessment of urban overheating impacts on human life. *Earth's Future*, *10*(8), e2022EF002682. https://doi.org/10.1029/2022EF002682
NOAA Climate.gov. (2023). *2022 global temperature recap (technical report)*. National Oceanic and Atmospheric Administration. Retrieved from https://www.climate.gov/news-features/understanding-climate/2022-global-temperature-recap
Obradovich, N., Migliorini, R., Mednick, S. C., & Fowler, J. H. (2017). Nighttime temperature and human sleep loss in a changing climate. *Science Advances*, *3*(5), e1601555. https://doi.org/10.1126/sciadv.1601555

Ohashi, Y., Genchi, Y., Kondo, H., Kikegawa, Y., Yoshikado, H., & Hirano, Y. (2007). Influence of air-conditioning waste heat on air temperature in Tokyo during summer: Numerical experiments using an urban canopy model coupled with a building energy model. *Journal of Applied Meteorology and Climatology*, *46*(1), 66–81. https://doi.org/10.1175/JAM2441.1

Oke, T. R., Mills, G., Christen, A., & Voogt, J. A. (2017). *Urban climates*. Cambridge University Press.

O'Neill, B. C., Tebaldi, C., van Vuuren, D. P., Eyring, V., Friedlingstein, P., Hurtt, G., et al. (2016). The scenario model intercomparison project (ScenarioMIP) for CMIP6. *Geoscientific Model Development*, *9*(9), 3461–3482. https://doi.org/10.5194/gmd-9-3461-2016

Oreskes, N., Shrader-Frechette, K., & Belitz, K. (1994). Verification, validation, and confirmation of numerical models in the earth sciences. *Science*, *263*(5147), 641–646. https://doi.org/10.1126/science.263.5147.641

Paramita, B., & Matzarakis, A. (2023). Urban biometeorology of tropical climate: Af, Am, Aw, a propensity of 34 provincial cities in Indonesia. In *Climate change and cooling cities* (pp. 283–296). Springer Nature Singapore.

Paranunzio, R., Dwyer, E., Fitton, J. M., Alexander, P. J., & O'Dwyer, B. (2021). Assessing current and future heat risk in Dublin city, Ireland. *Urban Climate*, *40*, 100983. https://doi.org/10.1016/j.uclim.2021.100983

Peel, M. C., Finlayson, B. L., & McMahon, T. A. (2007). Updated world map of the Köppen-Geiger climate classification. *Hydrology and Earth System Sciences*, *11*(5), 1633–1644. https://doi.org/10.5194/hess-11-1633-2007

Powers, J. G., Klemp, J. B., Skamarock, W. C., Davis, C. A., Dudhia, J., Gill, D. O., et al. (2017). The weather research and forecasting model: Overview, system efforts, and future directions. *Bulletin of the American Meteorological Society*, *98*(8), 1717–1737. https://doi.org/10.1175/bams-d-15-00308.1

Qiao, Z., Wang, N., Chen, J., He, T., Xu, X., Liu, L., et al. (2023). Urbanization accelerates urban warming by changing wind speed: Evidence from China based on 2421 meteorological stations from 1978 to 2017. *Environmental Impact Assessment Review*, *102*, 107189. https://doi.org/10.1016/j.eiar.2023.107189

Qin, S., Zhan, D., Geng, D., Peng, W., Tian, G., Shi, Y., et al. (2025). Modeling multivariable high-resolution 3D urban microclimate using localized fourier neural operator. *Building and Environment*, *273*, 112668. https://doi.org/10.1016/j.buildenv.2025.112668

Qin, Y., Liao, W., & Li, D. (2023). Attributing the urban–rural contrast of heat stress simulated by a global model. *Journal of Climate*, *36*(6), 1805–1822. https://doi.org/10.1175/jcli-d-22-0436.1

Ren, Z., Fu, Y., Dong, Y., Zhang, P., & He, X. (2022). Rapid urbanization and climate change significantly contribute to worsening urban human thermal comfort: A national 183-city, 26-year study in China. *Urban Climate*, *43*, 101154. https://doi.org/10.1016/j.uclim.2022.101154

Riahi, K., van Vuuren, D. P., Kriegler, E., Edmonds, J., O'Neill, B. C., Fujimori, S., et al. (2017). The shared socioeconomic pathways and their energy, land use, and greenhouse gas emissions implications: An overview. *Global Environmental Change*, *42*, 153–168. https://doi.org/10.1016/j.gloenvcha.2016.05.009

Robaa, S. (2006). A study of solar radiation climate at cairo urban area, Egypt and its environs. *International Journal of Climatology: A Journal of the Royal Meteorological Society*, *26*(13), 1913–1928. https://doi.org/10.1002/joc.1349

Robaa, S. M. (2013). Some aspects of the urban climates of greater Cairo region, Egypt. *International Journal of Climatology*, *33*(15), 3206–3216. https://doi.org/10.1002/joc.3661

Roth, M. (2007). Review of urban climate research in (sub)tropical regions. *International Journal of Climatology*, *27*(14), 1859–1873. https://doi.org/10.1002/joc.1591

Royé, D., Sera, F., Tobías, A., Hashizume, M., Honda, Y., Kim, H., et al. (2025). Short-term association between hot nights and mortality: A multicountry analysis in 178 locations considering hourly ambient temperature. *Environment International*, *203*, 109719. https://doi.org/10.1016/j.envint.2025.109719

Sadeghi, M., de Dear, R., Morgan, G., Santamouris, M., & Jalaludin, B. (2021). Development of a heat stress exposure metric–impact of intensity and duration of exposure to heat on physiological thermal regulation. *Building and Environment*, *200*, 107947. https://doi.org/10.1016/j.buildenv.2021.107947

Salamanca, F., Krpo, A., Martilli, A., & Clappier, A. (2010). A new building energy model coupled with an urban canopy parameterization for urban climate simulations: Part I. formulation, verification, and sensitivity analysis of the model. *Theoretical and Applied Climatology*, *99*(3), 331–344. https://doi.org/10.1007/s00704-009-0142-9

Salamanca, F., Martilli, A., Tewari, M., & Chen, F. (2011). A study of the urban boundary layer using different urban parameterizations and high-resolution urban canopy parameters with wrf. *Journal of Applied Meteorology and Climatology*, *50*(5), 1107–1128. https://doi.org/10.1175/2010jamc2538.1

Santamouris, M., Cartalis, C., Synnefa, A., & Kolokotsa, D. (2015). On the impact of urban heat island and global warming on the power demand and electricity consumption of buildings—A review. *Energy and Buildings*, *98*, 119–124. https://doi.org/10.1016/j.enbuild.2014.09.052

Schoetter, R., Caliot, C., Chung, T.-Y., Hogan, R. J., & Masson, V. (2023). Quantification of uncertainties of radiative transfer calculation in urban canopy models. *Boundary-Layer Meteorology*, *189*(1), 103–138. https://doi.org/10.1007/s10546-023-00827-9

Schupfner, M., Wieners, K. H., Wachsmann, F., Milinski, S., Steger, C., Bittner, M., et al. (2019). DKRZ MPI-ESM1.2-Hr model output prepared for CMIP6 ScenarioMIP [Dataset]. *Earth System Grid Federation*. https://doi.org/10.22033/ESGF/CMIP6.2450

Schupfner, M., Wieners, K. H., Wachsmann, F., Milinski, S., Steger, C., Bittner, M., et al. (2021). DKRZ MPI-ESM1.2-Lr model output prepared for CMIP6 ScenarioMIP [Dataset]. *Earth System Grid Federation*. https://doi.org/10.22033/ESGF/CMIP6.15349

Seland, Ø., Bentsen, M., Seland Graff, L., Olivié, D., Toniazzo, T., Gjermundsen, A., et al. (2019). NCC noresm2-lm model output prepared for CMIP6 ScenarioMIP [Dataset]. *Earth System Grid Federation*. https://doi.org/10.22033/ESGF/CMIP6.604

Semmler, T., Danilov, S., Rackow, T., Sidorenko, D., Barbi, D., Hegewald, J., et al. (2019). Awi awi-cm1.1mr model output prepared for CMIP6 ScenarioMIP [Dataset]. *Earth System Grid Federation*. https://doi.org/10.22033/ESGF/CMIP6.376

Seto, K. C., Güneralp, B., & Hutyra, L. R. (2012). Global forecasts of urban expansion to 2030 and direct impacts on biodiversity and carbon pools. *Proceedings of the National Academy of Sciences*, *109*(40), 16083–16088. https://doi.org/10.1073/pnas.1211658109

Shiogama, H., Tatebe, H., Hayashi, M., Abe, M., Arai, M., Koyama, H., et al. (2019). Miroc miroc6 model output prepared for CMIP6 ScenarioMIP [Dataset]. *Earth System Grid Federation*. https://doi.org/10.22033/ESGF/CMIP6.898

Shukla, K. K., & Attada, R. (2023). CMIP6 models informed summer human thermal discomfort conditions in Indian regional hotspot. *Scientific Reports*, *13*(1), 12549. https://doi.org/10.1038/s41598-023-38602-y

Siswanto, S., Nuryanto, D. E., Ferdiansyah, M. R., Prastiwi, A. D., Dewi, O. C., Gamal, A., & Dimyati, M. (2023). Spatio-temporal characteristics of urban heat Island of Jakarta metropolitan. *Remote Sensing Applications: Society and Environment*, *32*, 101062. https://doi.org/10.1016/j.rsase.2023.101062

Skamarock, W. C., & Klemp, J. B. (2008). A time-split nonhydrostatic atmospheric model for weather research and forecasting applications. *Journal of Computational Physics*, *227*(7), 3465–3485. https://doi.org/10.1016/j.jcp.2007.01.037

Smith, A., Lott, N., & Vose, R. (2011). The integrated surface database: Recent developments and partnerships. *Bulletin of the American Meteorological Society*, *92*(6), 704–708. https://doi.org/10.1175/2011bams3015.1

Solecki, W., Roberts, D., & Seto, K. C. (2024). Strategies to improve the impact of the ipcc special report on climate change and cities. *Nature Climate Change*, *14*(7), 685–691. https://doi.org/10.1038/s41558-024-02060-9
Strobl, C., Boulesteix, A. L., Zeileis, A., & Hothorn, T. (2007). Bias in random forest variable importance measures: Illustrations, sources and a solution. *BMC Bioinformatics*, *8*(1), 25. https://doi.org/10.1186/1471-2105-8-25
Sun, Y., Zhang, N., Ao, X., & Gao, Y. (2024). Numerical studies on the influence of building morphology on urban canopy wind speed. *Journal of Advances in Modeling Earth Systems*, *16*(6), e2023MS003881. https://doi.org/10.1029/2023ms003881
Swart, N. C., Cole, J. N., Kharin, V. V., Lazare, M., Scinocca, J. F., Gillett, N. P., et al. (2019a). Cccma CANESM5.1 model output prepared for CMIP6 ScenarioMIP [Dataset]. *Earth System Grid Federation*. https://doi.org/10.22033/ESGF/CMIP6.17199
Swart, N. C., Cole, J. N., Kharin, V. V., Lazare, M., Scinocca, J. F., Gillett, N. P., et al. (2019b). Cccma CANESM5 model output prepared for CMIP6 ScenarioMIP [Dataset]. *Earth System Grid Federation*. https://doi.org/10.22033/ESGF/CMIP6.1317
Takane, Y., Nakajima, K., & Kikegawa, Y. (2022). Urban climate changes during the COVID-19 pandemic: Integration of urban-building-energy model with social big data. *npj Climate and Atmospheric Science*, *5*(1), 44. https://doi.org/10.1038/s41612-022-00268-0
Taylor, K. E., Stouffer, R. J., & Meehl, G. A. (2012). An overview of cmip5 and the experiment design. *Bulletin of the American Meteorological Society*, *93*(4), 485–498. https://doi.org/10.1175/bams-d-11-00094.1
Teng, M., Duró Diaz, J. M., Mestres, E., Muela Castro, J., Lehmkuhl, O., & Rodriguez, I. (2025). Atmospheric boundary layer over urban roughness: Validation of large-eddy simulation. *Physics of Fluids*, *37*(6), 065129. https://doi.org/10.1063/5.0265556
Toparlar, Y., Blocken, B., Maiheu, B., & van Heijst, G. J. F. (2017). A review on the CFD analysis of urban microclimate. *Renewable and Sustainable Energy Reviews*, *80*, 1613–1640. https://doi.org/10.1016/j.rser.2017.05.248
UN DESA. (2018). *World urbanization prospects: The 2018 revision*. United Nations. Retrieved from https://www.un.org/development/desa/publications/2018-revision-of-world-urbanization-prospects.html
Varquez, A. C., Darmanto, N., Kawano, N., Takakuwa, S., Kanda, M., & Xin, Z. (2017). Representative urban growing scenarios for future climate models. *Journal of Japan Society of Civil Engineers, Series B1 (Hydraulic Engineering)*, *73*(4), I_103–I_108. https://doi.org/10.2208/jscejhe.73.I_103
Varquez, A. C., Kawano, N., Kanda, M., & Nakayoshi, M. (2018). Numerical investigation of anthropogenic heat emission impacts on large asian cities. *Journal of Japan Society of Civil Engineers, Series B1 (Hydraulic Engineering)*, *74*(5), I_1177–I_1182. https://doi.org/10.2208/jscejhe.74.5_i_1177
Varquez, A. C., Kiyomoto, S., Khanh, D. N., & Kanda, M. (2021). Global 1-km present and future hourly anthropogenic heat flux. *Scientific Data*, *8*(1), 64. https://doi.org/10.1038/s41597-021-00850-w
Varquez, A. C., Nakayoshi, M., & Kanda, M. (2015). The effects of highly detailed urban roughness parameters on a sea-breeze numerical simulation. *Boundary-Layer Meteorology*, *154*(3), 449–469. https://doi.org/10.1007/s10546-014-9985-4
Varquez, A. C. G., Darmanto, N. S., Honda, Y., Ihara, T., & Kanda, M. (2020). Future increase in elderly heat-related mortality of a rapidly growing Asian megacity. *Scientific Reports*, *10*(1), 9304. https://doi.org/10.1038/s41598-020-66288-z
Varquez, A. C. G., Kiyomoto, S., Khanh, D. N., & Kanda, M. (2020). Global 1-km present and future hourly anthropogenic heat flux (version 6) [Dataset]. *figshare*. https://doi.org/10.6084/m9.figshare.12612458.v6
Wang, M., Fu, X., Zhang, D., Chen, F., Liu, M., Zhou, S., & Tan, S. K. (2023). Assessing urban flooding risk in response to climate change and urbanization based on shared socio-economic pathways. *Science of the Total Environment*, *880*, 163470. https://doi.org/10.1016/j.scitotenv.2023.163470
Weeding, B., Love, P., Beyer, K., Lucieer, A., & Remenyi, T. (2024). High-resolution projections of outdoor thermal stress in the twenty-first century: A tasmanian case study. *International Journal of Biometeorology*, *68*(4), 777–793. https://doi.org/10.1007/s00484-023-02563-9
Weihs, P., Staiger, H., Tinz, B., Batchvarova, E., Rieder, H., Vuilleumier, L., & Jendritzky, G. (2012). The uncertainty of UTCI due to uncertainties in the determination of radiation fluxes derived from measured and observed meteorological data. *International Journal of Biometeorology*, *56*(3), 537–555. https://doi.org/10.1007/s00484-011-0416-7
WRF Model Development Team. (2024). WRF version 4.6.0 [Software]. *GitHub*. Retrieved from https://github.com/wrf-model/WRF/releases/tag/v4.6.0
Wu, F., Yang, X., & Shen, Z. (2019). Regional and seasonal variations of outdoor thermal comfort in China from 1966 to 2016. *Science of the Total Environment*, *665*, 1003–1016. https://doi.org/10.1016/j.scitotenv.2019.02.190
Yamanaka, M. D. (2016). Physical climatology of Indonesian maritime continent: An outline to comprehend observational studies. *Atmospheric Research*, *178*, 231–259. https://doi.org/10.1016/j.atmosres.2016.03.017
Yamato, H., Mikami, T., & Takahashi, H. (2017). Impact of sea breeze penetration over urban areas on midsummer temperature distributions in the tokyo metropolitan area. *International Journal of Climatology*, *37*(15), 5154–5169. https://doi.org/10.1002/joc.5152
Yuan, J., Lin, Q., Chen, S., Zhao, H., Xie, X., Cai, Z., et al. (2022). Influence of global warming and urbanization on regional climate of megacity: A case study of chengdu, China. *Urban Climate*, *44*, 101227. https://doi.org/10.1016/j.uclim.2022.101227
Yukimoto, S., Koshiro, T., Kawai, H., Oshima, N., Yoshida, K., Urakawa, S., et al. (2019). MRI MRI-ESM2.0 model output prepared for CMIP6 ScenarioMIP [Dataset]. *Earth System Grid Federation*. https://doi.org/10.22033/ESGF/CMIP6.638
Zhang, J., You, Q., Ren, G., Ullah, S., Normatov, I., & Chen, D. (2023). Inequality of global thermal comfort conditions changes in a warmer world. *Earth's Future*, *11*(2), e2022EF003109. https://doi.org/10.1029/2022EF003109
Zhao, C., Lin, Z., Yang, L., Jiang, M., Qiu, Z., Wang, S., et al. (2025). A study on the impact of meteorological and emission factors on pm2.5 concentrations based on machine learning. *Journal of Environmental Management*, *376*, 124347. https://doi.org/10.1016/j.jenvman.2025.124347
Zhao, L., Oleson, K., Bou-Zeid, E., Krayenhoff, E. S., Bray, A., Zhu, Q., et al. (2021). Global multi-model projections of local urban climates. *Nature Climate Change*, *11*(2), 152–157. https://doi.org/10.1038/s41558-020-00958-8
Zhao, Q., Meng, Q., Gao, L., & Zhu, M. (2025). Fu3d: The first global projections of future urban three-dimensional (3D) expansion for the 21st century under shared socioeconomic pathways. *Scientific Data*, *12*(1), 1555. https://doi.org/10.1038/s41597-025-05711-4
Zhao, Y., Zhong, L., Ma, Y., Fu, Y., Chen, M., Ma, W., et al. (2021). Wrf/ucm simulations of the impacts of urban expansion and future climate change on atmospheric thermal environment in a Chinese megacity. *Climatic Change*, *169*(3), 38. https://doi.org/10.1007/s10584-021-03287-7
Zhou, J., Zhang, X., Xie, J., & Liu, J. (2023). Effects of elevated air speed on thermal comfort in hot-humid climate and the extended summer comfort zone. *Energy and Buildings*, *287*, 112953. https://doi.org/10.1016/j.enbuild.2023.112953
Ziehn, T., Chamberlain, M., Lenton, A., Law, R., Bodman, R., Dix, M., et al. (2019). CSIRO ACCESS-ESM1.5 model output prepared for CMIP6 ScenarioMIP [Dataset]. *Earth System Grid Federation*. https://doi.org/10.22033/ESGF/CMIP6.2291